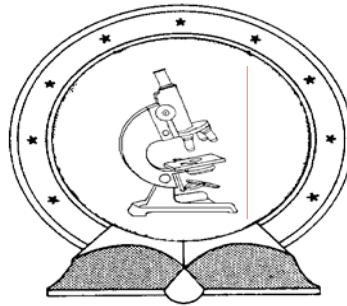


DE TTK



1949

**Elastic and dissipative energies in phase transformations of
Cu-based shape memory alloys**

PhD Thesis

Tarek Yousif AbdelRaouf El Rasasi

Supervisor

Prof. Dezső Beke

University of Debrecen

PhD School in Physics

Debrecen

2012

Prepared at
the University of Debrecen
PhD School in Physics
and
The Department of Solid State Physics

Ezen értekezést a Debreceni Egyetem Fizikai Tudományok Doktori Iskola Szilárdtestfizika és Anyagtudomány programja keretében készítettem a Debreceni Egyetem Természettudományi Doktori Tanácsa (PhD) fokozatának elnyerése céljából.

Debrecen, 2012.

Tarek Elrasasi

Tanúsítom, hogy Tarek Elrasasi doktorjelölt 2008 -2012 között a fent megnevezett doktori iskola szilárdtest fizika és anyagtudomány programjának keretében irányításommal végezte munkáját. Az értekezésben foglalt eredményekhez a jelölt önálló alkotó tevékenységével meghatározóan hozzájárult. Az értekezés elfogadását javasolom.

Debrecen, 2012.

Dr. Beke Dezső

Supervisor

**Elastic and dissipative energies in phase transformations of Cu-based
shape memory alloys**

Értekezés a doktori (Ph.D.) fokozat megszerzése érdekében a
.....**Fizika**..... tudományágban

Írta: **Tarek Y. Elrasasi**.. okleveles**Fizikus**.....

Készült a Debreceni Egyetem**Fizikai Tudományok**..... doktori iskolája
(**Szilárdtestfizika és Anyagtudomány programja**) keretében

Témavezető: **Dr. Beke Dezső** .

A doktori szigorlati bizottság:

elnök: Dr.
tagok: Dr.
Dr.....

A doktori szigorlat idipontja: 20.....

Az értekezés bírálói:

Dr.....
Dr.....

A bírálóbizottság:

elnök: Dr.
tagok: Dr.
Dr.....
Dr.....
Dr.....

Az értekezés védésének idipontja: 2012.....

Contents

Contents	1
List of symbols	4
Introduction	6
Aim of my work	7
Chapter I: Shape memory alloys	8
I.1 Active materials.....	8
I.2 Shape memory alloys.....	9
I.3 Martensitic transformation.....	9
I.4 Basic thermodynamics of martensitic transformations.....	11
I.5 Terminology.....	13
I.5.1 Shape memory effect.....	13
I.5.2 Two-way shape memory effect.....	14
I.6 Typical shape memory alloys.....	15
I.7 SMAs Applications.....	15
I.7.1 Aerospace.....	15
I.7.2 Medical.....	17
I.7.3 Other industrial applications.....	17
I.7.4 Consumer Products.....	18
I.8 Magnetic shape memory alloys.....	18
References.....	19
Chapter II: Theoretical Background	20
II.1 Introduction.....	20
II.2 Model of thermoelastic martensitic transformations.....	21

IV.1.3 Analysis of the results obtained from σ - ε	
hysteresis loops.....	49
IV.1.4 Relations between the start and finish stresses	
and test temperature.....	51
IV.1.5 Self-consistency of our analysis.....	53
IV.1.6 Stress and temperature dependence of the total dissipative	
and elastic energy (D and E, respectively).....	54
IV.1.6.1 stress dependence.....	54
IV.1.6.2 thermal dependence.....	57
IV.1.7 Dependence of the dissipative and elastic energies	
on the number of cycles.....	58
IV.1.7.1 Thermal cycling.....	58
IV.1.7.2 Mechanical cycling.....	60
IV.2. Result on polycrystalline samples.....	61
References.....	63
V. Summary.....	64
Magyar nyelvű összefoglaló.....	68
List of publications.....	71
Citations.....	71
Posters.....	72
Appendices.....	73
Appendix 1	73
Acknowledgments.....	74

List of symbols and abbreviations

SMA _s	shape memory alloys
A	austenitic phase
M	martensitic phase
T	temperature
M _s	martensite start temperature
M _f	martensite finish temperature
A _s	austenite start temperature
A _f	austenite finish temperature
σ	applied uniaxial stress
σ_{ms}	start martensite stress
σ_{mf}	finish martensite stress
σ_{As}	start austenite stress
σ_{Af}	finish austenite stress
DSC	differential scanning calorimeter
ξ	martensite volume fraction
G _c	chemical Gibbs free energy
g _c	derivative of the chemical Gibbs free energy by ξ
G _{nch}	non chemical Gibbs free energy
G _c ^M	chemical Gibbs free energy of martensite phase
G _c ^A	chemical Gibbs free energy of austenite phase
T ₀	the equilibrium temperature
ΔU_c	difference of the internal energy of the martensite and austenite phases, $\Delta U_c = U_c^M - U_c^A$
Δu_c	derivative of the ΔU_c by ξ
ΔS_c	entropy change, $\Delta S_c = S_c^M - S_c^A$
Δs_c	derivative of the ΔS_c by ξ
D	total dissipative energy
E	total elastic energy
d	derivative of the total dissipative energy by ξ
d ₀	dissipative energy contribution in the austenite phase (at $\xi = 0$)
d ₁	dissipative energy contribution in the martensite phase (at $\xi = 1$)

e	derivative of the total elastic energy by ξ
e_0	elastic energy contribution in the austenite phase (at $\xi = 0$)
e_1	elastic energy contribution in the martensite phase (at $\xi = 1$)
B	magnetic field
p	pressure
M	magnetization
V	molar volume
ε^r	transformation strain
Q	heat of transformation
C_A	heat capacity of austenite
C_m	heat capacity martensite
R	resistance
η	volume ratio of the stress induced (single) variant martensite

Introduction

The amazing shape memory property of shape memory alloys (*SMA*s) attracted the attention of many scientists and engineers in the last decades, because of a wide range of important technical applications. Many models have been published for the description of the shape memory property as well as for the determination of critical parameters important for the technology. Furthermore, many experiments have also been carried out to understand the basic mechanisms and the details of the shape memory effect (*SME*).

In my thesis - after an introduction containing the most important definitions, notations and terminologies - I will describe in details one of these models (developed in Debrecen) and use it for analysis of the experimental results obtained in Cu based single and polycrystalline samples (CuAl(11.5wt%)Ni(5.0wt%) and CuAl(11,6wt%)Be(0.36wt%) respectively). By using this model I was able to calculate the non chemical (elastic and dissipative) free energy terms and their contributions to the martensite/austenite phase transformation and could also obtain the stress and temperature dependence of these energies. Furthermore, I also determined the dependence of the above energies on the number of thermal as well as mechanical cycles.

Aim of my work

Experimental investigation of thermal and stress induced martensitic transformations in single and polycrystalline Cu-based shape memory alloys. Using the model developed in Debrecen, carry out the separation of the non-chemical energy contributions (dissipative and elastic energies) from the free energy of the transformation. Determining how the dissipative and elastic energies depend on the stress and temperature as well as on the number of the thermal and mechanical cycles. Since in the interpretation of data obtained, the stress and temperature dependence of the transformation strain has a central role, these functions also have to be determined experimentally.

My work was

- Finding the full transformation strain as the function of temperature (for mechanically induced transformation) and stress (for thermally induced transformations). Determining the start and finish temperatures as well as start and finish stresses in the martensite transformations as a function of temperature and stress, and the effect of the contribution of the elastic energy on these parameters;
- Studying the stress and temperature dependence of the dissipative and elastic energies;
- Studying the effects of the thermal and mechanical cycling on the elastic and dissipative energies.

Chapter I

Shape memory alloys

This chapter summarizes the most important definitions, notations, terminologies and typical examples of application of shape memory alloys.

I.1 Active materials

In the last few decades the demand for lighter, stronger materials with tailored properties addressing stringent structural requirements and providing additional engineering functionality (e.g., sensing, actuation, electromagnetic shielding) has created a new branch of materials called *multifunctional materials*. A specific subgroup of multifunctional materials exhibiting sensing and actuation capabilities is known as *active materials*. Active materials in general exhibit a mechanical response when subjected to a non mechanical field (thermal, electrical, magnetic, etc.; see Fig. I.1.). Examples of active materials are *piezoelectric* and *electrostrictive* (coupling of mechanical and electric fields), *piezomagnetic* and *magnetostrictive* (coupling of mechanical and magnetic fields) materials and *shape memory alloys* [I.1].

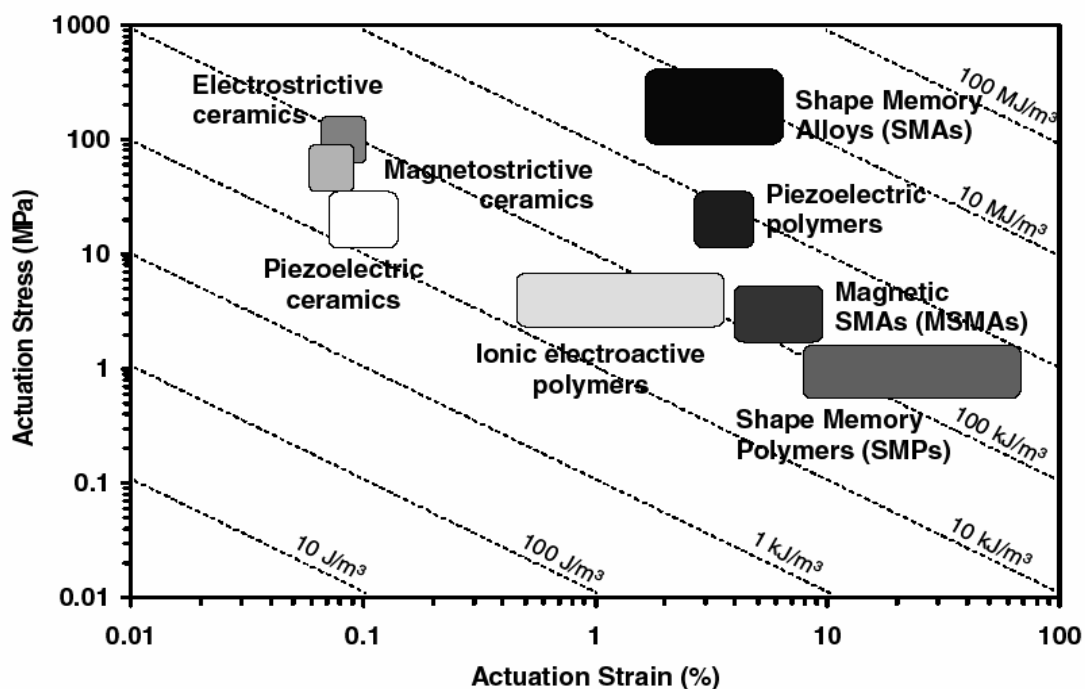


Fig. I.1. Actuation stress-strain diagram for active materials [I.1].

I.2 Shape memory alloys

Shape Memory Alloys (*SMAs*) form a unique class of alloys with ability to remember their original shape and returning back to the pre-deformed shape by heating, even under high load, i.e. they can be used as actuators. Furthermore, *SMAs* can be used as vibration damping units absorbing and dissipating mechanical energy. In the last few decades many publications have been devoted to the understanding of their properties, microstructural behaviour and their industrial applications [I.1, I.2].

I.3 Martensitic transformation

SMAs have two phases with two different crystal structures; the *austenitic phase (A)* at high temperature - it is called as parent phase as well - and the *martensitic phase (M)* at low temperature. The transformation from one phase to the other is diffusionless, i.e. takes place by the change of the crystal structure by short local rearrangements of atoms [I.3]. This transformation is called martensitic phase transformation (Fig.I.2.).

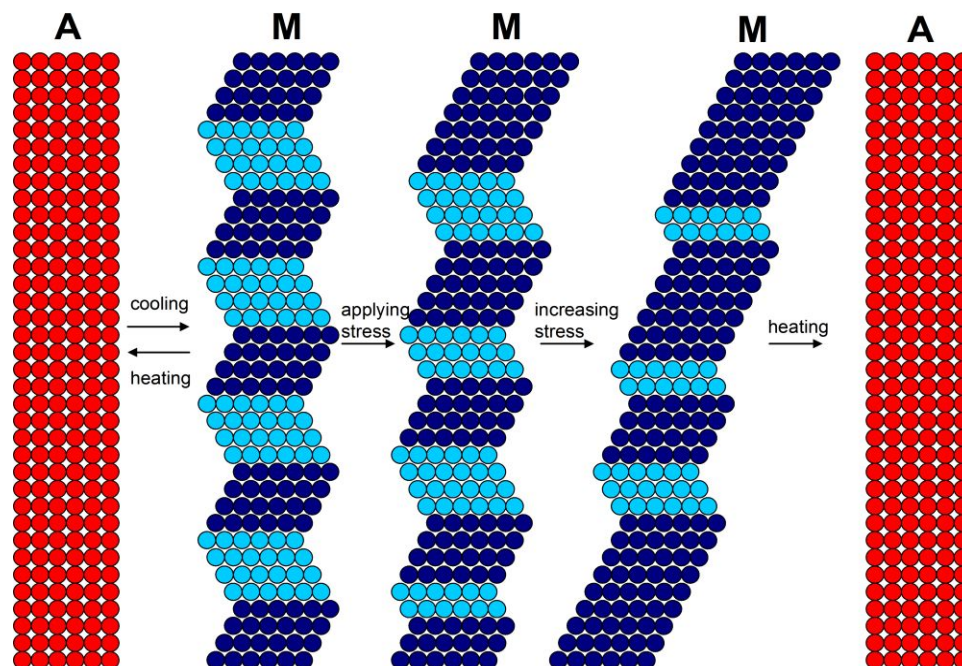


Fig. I.2. Phase change during *A/M* (and *M/A*) transformation: the first step is the development of multivariant martensite structure. In the second and third steps the application of the stress results in the rearrangement of the variant structure (approaching to a single variant structure) with large shape change. During the last step (*M/A* transformation) the original shape is recovered. This is the so-called one-way shape memory effect.

Usually the austenite phase has cubic (high symmetry) structure, whereas the martensite structure may be tetragonal, orthorhombic or monoclinic (with low symmetry). The martensite phase can be formed in crystallographically equivalent but differently oriented regions: these are called variants. During the A/M phase transformation - without applying any external stress - randomly oriented multivariant (or twinned) martensite structure develops with small or negligible shape change (Figs. I.2. and I.3.).

Fig. I.3. shows the transformation from one phase to the other phase showing the four characteristic temperatures associated with the phase transformation. From the martensite to the austenite phase (by heating up) the austenite starts at A_s and finishes at A_f . Similarly, from the austenite to the martensite phase (by cooling down) the martensite phase starts at M_s and finishes at M_f .

These transformation temperatures can be determined by measuring certain physical properties, such as the absorbed and released heat in DSC, resistance, elongation, etc., as the function of temperature.

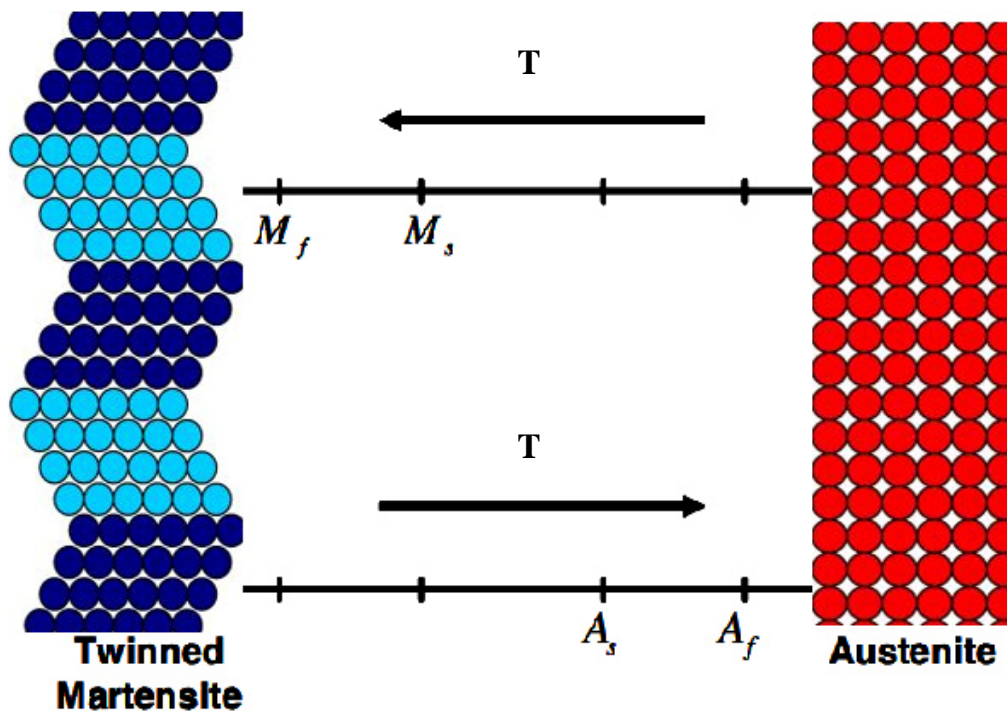


Fig. I.3. Thermally induced phase transformation.

The change from one phase to another can be triggered not only thermally but also by applying mechanical stress. At fixed temperature, by increasing the applied stress there will be a phase transformation from austenite to martensite, with single

variant structure (Fig. I.4.) having a visible change in the shape of sample. In the literatures, four characteristic stresses are used; start and finish of martensite, σ_{ms} and σ_{mf} , and start and finish of austenite, σ_{As} and σ_{Af} , respectively (see Fig. I.4.).

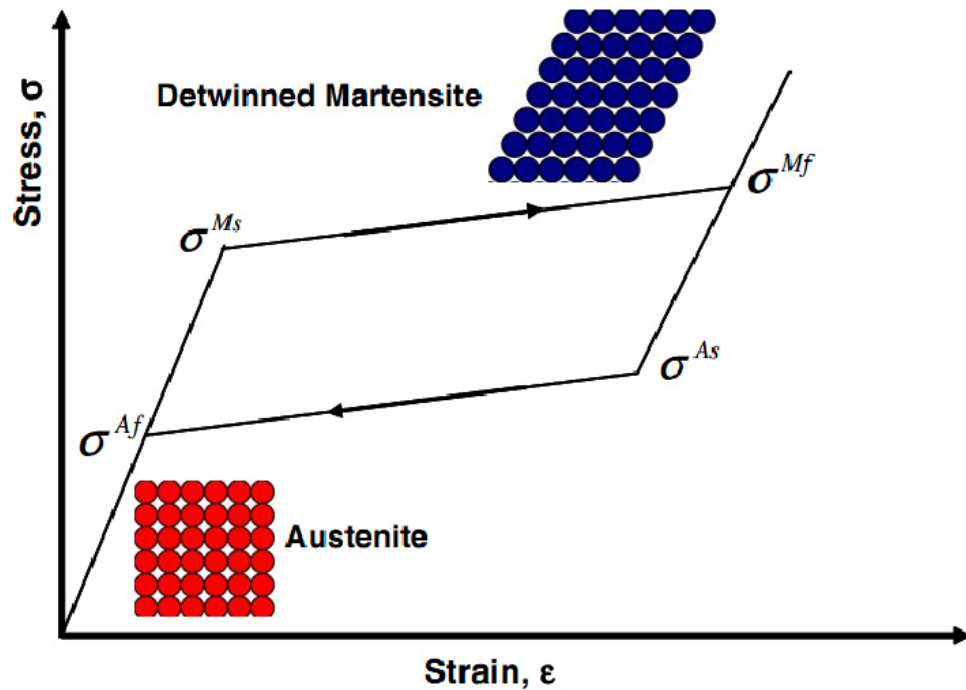


Fig. I.4. Mechanically induced phase transformation [I.1].

I.4 Basic thermodynamics of martensitic transformations

Because there is no change in the composition during the martensitic transformation, the chemical Gibbs free energy can be plotted as a function of the temperature as shown in Fig. I.5. T_0 is the equilibrium temperature where the chemical Gibbs free energies of the martensite and austenite phases (G_c^M and G_c^A , respectively) are equal to each other. At this point

$$\Delta G_c = G_c^M - G_c^A = \Delta U_c - T_0 \Delta S_c = 0 \quad (\text{I.1})$$

where ΔU_c and ΔS_c denote the internal energy and entropy change of the transformation, respectively.

In general the total change of the Gibbs free energy (i.e taking also into account the elastic and dissipative energy contributions) can be given as:

$$\Delta G_t = \Delta G_c + \Delta G_{nc} = \Delta G_c + (D + E). \quad (I.2)$$

Here $\Delta G_c = (T_o - T)\Delta S_c$ chemical term is the driving force for the transformation (and it is negative for $T < T_o$ because $\Delta S_c = S_c^M - S_c^A < 0$: see also Fig. I.5), and D and E denote the dissipative and elastic energy, respectively. The dissipative energy is due to the frictional motion of the interfaces, while the elastic energy accumulated/released because of the overlapping of elastic fields of the different martensite nuclei and/or variants. Thus, the elastic energy is positive for the $A \rightarrow M$ transformation and negative for the reverse direction. On the other hand, the dissipative energy is positive for both directions [I.4].

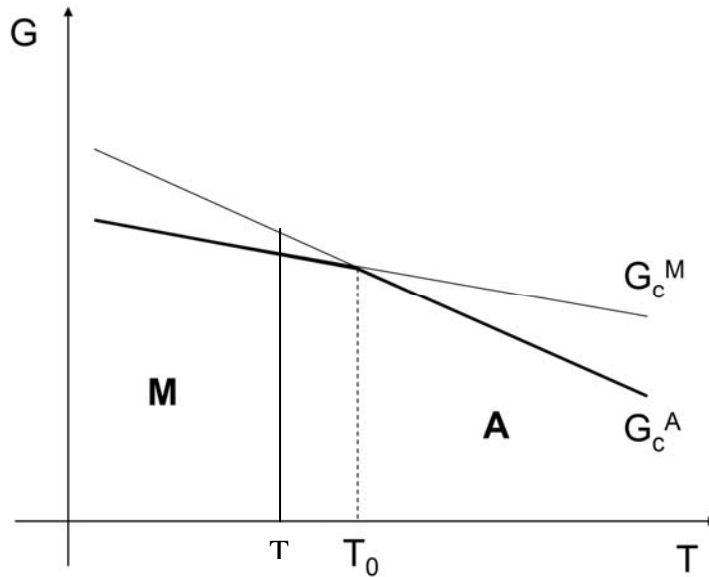


Fig. I. 5. Temperature dependence of the chemical Gibbs free energies and the position of the equilibrium transformation temperature.

It is clear from Fig. I.5. and eq. (I.2) that at a certain temperature below T_o (here ΔG_c is negative and both D and E are positive). ΔG_t will be zero when the chemical and non-chemical terms have the same absolute value. From this point the particle formed can grow further or become smaller only by undercooling or overheating, respectively (balance between the chemical and non-chemical terms).

I.5 Terminology

I.5.1 Shape memory effect

*SMA*s exhibit the shape memory effect (*SME*) when they are deformed in the martensitic phase and then unloaded at a temperature below A_s . The reversible shape change, leading to a large elastic deformation, is due to the stress induced phase transformation as it is illustrated in Fig. I.4. This behaviour is called **super or pseudo elasticity**.

If one applies uniaxial stress on the material in martensitic state just after cooling down from austenite, then the firstly formed randomly oriented martensite variant structure will be rearranged to the single variant structure with high plastic deformation, which can be as large as about 6% (see the first three steps in Fig. I.2.). This deformation remains even if one removes the stress. This is the so called **super-plastic behaviour**, during which there is only a very moderate dislocation activity (which is typical in common plasticity).

If the material deformed in martensitic phase is heated above A_f , it will retain to its original shape by transforming back into the parent austenitic phase (see also Fig. I.6.). This is the **one-way shape memory effect**.

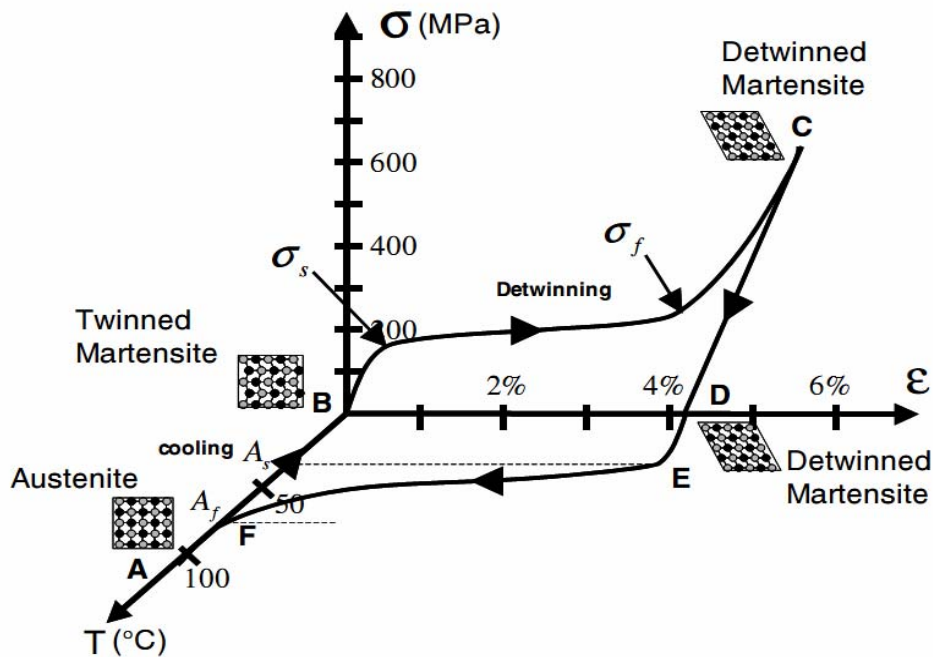


Fig. I.6. Stress - strain - temperature diagram for NiTi *SMA* [I.1].

I.5.2 Two-way shape memory effect

In the case, schematically illustrated in Fig. I.2., only the shape of the austenite phase is remembered. But, it is also possible to remember the shape of the martensitic phase under certain conditions. For example repeating many times the subsequent steps shown on Fig. I.2. it happens that during a next heating martensite variants mainly belonging to the single variant structure (see the shape after the third step) will develop and thus, after such a “learning process”, the sample will change its shape in each cycle. This is **the two way shape memory effect**. The reason why the specimen remembers the shape of the martensite phase too can be explained as follows. Upon heavy deformation in martensite phase, some dislocations are also introduced and these dislocations can still exist even in the austenite phase after heating [I.5]. In the next cooling step the presence of these dislocations can help the nucleation of those variants of the martensite which existed just before the heating.

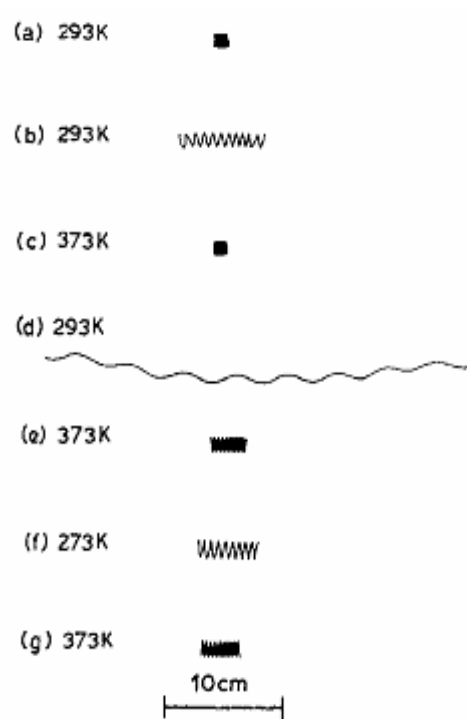


Fig. I.7. Shape memory effect and the two way shape memory effect in TiNi.

Fig. I.7. illustrates the learning process and the two way shape memory behaviour. When the applied stress (and strain) in the martensitic state (b) is relatively small, the specimen reverts to the original shape completely (steps a-c). However, when the applied stress is large (d), irreversible slips also occur, and the shape does not revert to the original one even after heating above A_f , [(c) and (e)]. In the next cooling cycle, the specimen elongates automatically as shown in (f). Then, if heating and cooling is repeated, the specimen changes its shape between (g) and (f), respectively.

I.6 Typical shape memory alloys

Several alloys have been developed that display varying degrees and types of shape memory behavior. The most commercially successful have been Ni–Ti, Ni–Ti–X and Cu-based alloys [I.6, I.7], Ni–Ti and ternary Ni–Ti–X alloys are used in more than 90% of new *SMA* applications. Ni–Ti alloys are more expensive than copper alloys, but they are preferred for their ductility, stability in cyclic applications, corrosion resistance, biocompatibility, and higher electrical resistivity for resistive heating in actuator applications. The most common Cu-based alloys, Cu–Al–Ni, Cu–Zn–Al, and Cu–Al–Be are used for their narrow thermal and adaptability to two-way memory training [I.8].

I.7 SMA's Applications

Because of the amazing properties of the *SMA*s, there are lots of applications from aerospace industry to consumer products.

I.7.1 Aerospace

Many of the initial ideas for production and applications of *SMA*s were pioneered in the aerospace industry. *SMA* materials are used to take advantage of properties such as high power-to-mass ratios and ideal actuating behavior in zero-gravity conditions. Designs that use these properties replace heavier, more complex conventional devices because of reduced weight, design simplicity, and reliability.

- **Cryofit Hydraulic Pipe Couplings**

SMA couplings were one of the first successful commercial applications of *SMA*s. In 1969, Raychem Corporation introduced shrink-to-fit hydraulic pipe couplings for F-14 jet fighters. This coupling is fabricated from a Ni–Ti–Fe alloy whose martensitic transformation temperature is below -120°C . It is machined at room temperature to an inner diameter approximately 4% smaller than the outer diameter of the piping designed to join. When cooled below -120°C , the coupling is forced to a diameter 4% greater than the pipe diameter

for an overall internal strain of about 8%. When warmed up, the coupling diameter decreases to form a tight seal between the pipes.



Fig. I.8. *SMA* devices. Clockwise from top left: memory card ejector mechanism for laptop computers; Cryofit hydraulic pipe couplings; Cryocon electrical connector; fire safety lid release for public garbage receptacles [I.8].

- **Mars Sojourner Rover Actuator**

SMA Ni–Ti wire was used to actuate a glass plate above a small solar cell on the Rover unit during the Pathfinder/Sojourner mission to Mars. A material adhesion experiment performed during the mission used the actuator to replace large, heavy motors and solenoids.

- **Smart Airplane Wings**

Composite structures that have *SMA* wires embedded can be used to change the shape of an airplane wing. The embedded wires may be activated to constrict and improve the vibrational characteristics of the wing, heated to change their effective modulus to reduce vibration, or activated to alter the shape of the wing for optimal aerodynamics. All of these properties can be

used to produce an adaptive airplane wing that alters as environmental conditions change to improve efficiency and reduce noise.

I.7.2 Medical

Because of its excellent biocompatibility (except for some persons having Ni allergy) and corrosion resistance, Ni–Ti has been used in many successful medical devices and is now widely accepted throughout the medical industry.

- **Orthodontic Dental Arch Wires**
- **Orthopedic Devices**

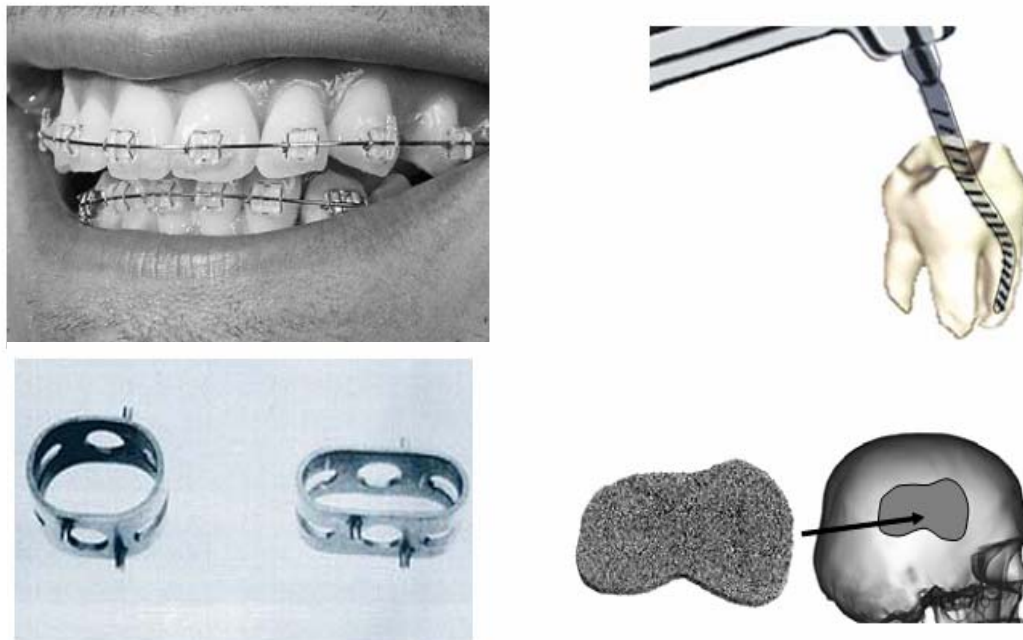


Fig. I.9. Medical application of *SMAs* [I.1].

I.7.3 Other industrial applications

SMAs applications for the automotive industry are challenging for two primary reasons: the extreme range of operating temperatures expected during use and the market demand for low-cost components. Some of the applications are like; Pressure Control Governor Valve, Toyota Shape-Memory Washer, Rock Breakers, Heat Engines ... etc.

I.7.4 Consumer Products

Nowadays, *SMA*s are used everywhere in our life here some of these applications

- Robotic Doll
- Miscellaneous Products
- Nicklaus Golf Clubs
- Recorder Pen Mechanism
- Superelastic eyeglass frames
- Portable Phone Antennae
- Greenhouse Window Opener
- Rice Cooker Valve.



Fig. I.10. Other applications of *SMA*s [I.1].

I.8 Magnetic shape memory alloys

The martensitic phase transformation can also be triggered by applying external magnetic field in some ferromagnetic alloys *SMA*s such as Ni_2MnGa and Co_2NiAl [I.5, I.9]. The strain can be up to 10%. This big strain is due to the reorientation of the martensitic variants to one preferred variant according to the magneto-elastic coupling between the martensite variants and magnetic domains: the magnetic field tends arrange the magnetic domains and their rearrangement is coupled to the rearrangement of the martensite variant structure too. The frequency of the actuation is very high – can be even in the kHz range - because here the driving force is the magnetic field and not the change of the temperature.

References

- [I.1] Dimitris C. Lagoudas (Ed) . *Shape Memory Alloys*, Springer Science+Business Media, LLC, (2008).
- [I.2] J. Rodriguez-Aseguinoza, I. Ruiz-Larrea, M.L. No, A. Lopez-Echarri, J. San Juan, *Acta Mater.* 56 (2008) 6283.
- [I.3] R.W Cahn, and P. Hasen (Eds). *Physical Metallurgy*, North Holland, Amsterdam,(1996).
- [I.4] Z. Palánki, L. Daróczy, D.L. Beke, *Mater. Trans.*, A46 (2005) 978.
- [I.5] K. OTSUKA and C.M Wayman *Shape memory materials*, Cambridge University Press, (1998).
- [I.6] K. Otsuka, X. Ren, *Prog. Mater. Sci.*, 50 (2005) 511.
- [I.7] A. Planes, T. Castan, J. Ortin, L. Delay, *J Appl. Phys.* 66(6) (1989) 2342.
- [I.8] Mel Schwartz. *Encyclopaedia of smart materials*, John Wiley and Sons, Inc, (2002).
- [I.9] Z. Palánki, L. Daróczy, L. Harasztosi D.L. Beke, T. A. Lograsso , D.L. Schlagel, *Mater. Trans.*, 47,No. 3 (2006) 631.

Chapter II

Theoretical Background

In this chapter, I will describe in details of the model (Beke-Daroczi) [II.1-II6] used, i.e. the way of the determination of non-chemical (elastic and dissipative) energy terms from the experimental data.

II.1 Introduction

Since the discovery of the martensite/austenite transformation by the German metallurgist *Adolf Martens* (1850–1914), many models have been published about the determination of the characteristic parameters such as T_0 (equilibrium transformation temperature, at which the chemical free energies of the two phases equals)) and the elastic and the dissipative energies belonging to the phase transformation.

There is a long standing debate in the literature that while the contribution of the dissipative energy, D , to the austenite/martensite, A/M , (or reverse, M/A) transformation can be directly obtained from the experimental data (thermal hysteresis loop, mechanical hysteresis loop, DSC curves), the contributions from the elastic, E , and the chemical free energy, ΔG_c , can not be separated. Since the temperature dependence of ΔG_c is described by $\Delta G_c = \Delta U_c - T\Delta S_c = (T - T_0)\Delta S_c$, where $\Delta S_c = \Delta U_c / T_0$ (see also below) is the entropy change of the phase transformation, the separation of E and ΔG_c would need the knowledge of ΔS_c and T_0 . While the direct determination of ΔS_c is possible (e.g. from the measured DSC curves [II.7]) the determination of T_0 is rather difficult. It has been shown that the simple expression proposed by Tong and Waynman [II.8]: $T_0 = \frac{M_s + A_f}{2}$ (where M_s and A_f are the martensite start and austenite finish temperatures respectively) can not be valid in general. Salzbrenner and Cohen [II.9] have illustrated that this expression is valid only if the elastic energy contributions to M_s and A_f can be neglected.

II.2 Model of thermoelastic martensitic transformations

Martensitic transformations, as first order phase transformations with hysteresis loops, can take place in both directions (i.e. austenite/martensite, A/M , and reverse M/A) [II.10]. During such a transformation the change of the Gibbs free energy per mole can be written e.g. as [II.11, II.12] (if we neglect the interface term for nucleation):

$$\Delta G^\downarrow = G^M - G^A = \Delta G_c^\downarrow + E^\downarrow + D^\downarrow. \quad (\text{II.1})$$

Obviously a similar expression can be written for the $A \rightarrow M$ transformation as well, using the index \uparrow . Here ΔG_c^\downarrow is the change in the *chemical* Gibbs-free energy. E^\downarrow and D^\downarrow are the elastic and dissipative energies, respectively.

The elastic energy accumulates as well as releases during the down and up processes just because the formation of differently oriented nuclei/variants of the martensite phase is usually accompanied by a development of an elastic energy field (due to the overlapping of transformation strains of different nuclei). It is usually supposed that $E^\downarrow = -E^\uparrow > 0$. The dissipative energy is always positive in both directions. In principle, one more additional term, proportional to the entropy production, should be considered, but it can be supposed [II.13] that for thermoelastic transformations all the energy losses are mechanical works, which are dissipated without entropy production, i.e. the dissipation is mainly energy relaxation in the form of elastic waves. Indeed acoustic waves were detected as acoustic emissions during the transformation. Thus in the following the term proportional to the entropy production will be neglected. Furthermore, usually there is also a nucleation term on the right hand side of (II.1), proportional to the interface energy between the two phases. However, since this term, similarly to the dissipative energy, is positive in both directions and thus it is difficult to separate from D , it can be considered to be included in the dissipative term.

Let us denote the martensite (volume) fraction by ξ . The transformation temperature T_0 (at which the two phases are in equilibrium for a given ξ) can be given as:

$$\frac{\Delta G^\downarrow}{\partial \zeta} = \frac{\Delta G_c^\downarrow}{\partial \zeta} + \frac{\Delta E}{\partial \zeta} + \frac{\Delta D}{\partial \zeta} = \Delta g_c + e^\downarrow(\zeta) + d^\downarrow(\zeta) = 0 \quad (\text{II.2})$$

where it is assumed that Δg_c^\downarrow is independent of ξ and

$$\Delta g_c^\downarrow = \Delta u_c^\downarrow - T \Delta s_c^\downarrow, \quad (\text{II.3})$$

with $\Delta u_c^\downarrow = u^M - u^A (<0)$ and $\Delta s_c^\downarrow = s^M - s^A (<0)$ (the M phase is the low temperature phase). Furthermore, at the “equilibrium transformation temperature”, T_0 (the temperature of zero-change in the chemical free energy)

$$\Delta g_c^\downarrow(T_0) = 0, \text{ i.e. } T_0 = \frac{\Delta u_c^\downarrow}{\Delta s_c^\downarrow} = \frac{\Delta u_c^\uparrow}{\Delta s_c^\uparrow} \quad (\text{II.4})$$

and e.g. at any temperature different from T_0

$$\Delta g_c^\downarrow(T) = (T_0 - T) \Delta s_c^\downarrow. \quad (\text{II.5})$$

If $T < T_0$ then there is an under-cooling and $\Delta g_c^\downarrow(T)$ is negative.

In thermoelastic transformations the elastic term plays a determining role. For example at a given under-cooling, when the elastic term will be equal to the chemical one, for the further growth of the martensite an additional under-cooling is required. Thus, if the sample is further cooled the M phase grows further, while if the sample is heated it becomes smaller. Indeed, in *thermoelastic* materials it was observed that once a particle formed and reached a certain size its growth stops and grows further or decreases with increasing or decreasing the temperature. This is *the thermoelastic behaviour* (the thermal and elastic terms are balanced).

II.2.1 Thermal hysteresis loop

Starting from (II.2) and (II.3), introducing the notation $\Delta s = \Delta s_c^\downarrow = -\Delta s_c^\uparrow (<0)$, as well as taking the assumptions usual in the treatment of thermoelastic transformations

(in accordance with the signs of E and D): $e(\xi)=e^\downarrow(\xi)=-e^\uparrow(\xi)$ as well as $d(\xi)=d^\downarrow(\xi)=d^\uparrow(\xi)$, one can arrive at the following relations [II.3,II.6]

$$T^\downarrow(\zeta)=T_0-\frac{d(\zeta)+e(\zeta)}{-\Delta s} \quad (\text{II.6.a})$$

$$T^\uparrow(\zeta)=T_0+\frac{d(\zeta)-e(\zeta)}{-\Delta s} \quad (\text{II.6.b})$$

Thus, by taking the sum as well as the difference of $T^\uparrow(\xi)$ and $T^\downarrow(\xi)$ one can get the $e(\xi)$ and $d(\xi)$, respectively from:

$$T^\uparrow(\zeta)-T^\downarrow(\zeta)=\frac{2d(\zeta)}{-\Delta s} \quad (\text{II.7})$$

and

$$T^\uparrow(\zeta)+T^\downarrow(\zeta)=\frac{2T_0-2e(\zeta)}{-\Delta s} \quad (\text{II.8})$$

The inverses of (II.6a) and (II.6b), i.e. the $\xi(T^\downarrow)$ and $\xi(T^\uparrow)$ functions, are the down and up branches of the thermal hysteresis loops. The martensite (austenite) start, M_S (A_S) and finish, M_f , A_f temperatures can be obtained from (II.6a) (and (II.6b)), respectively taking them at $\xi = 0$ as well as $\xi = 1$ (See Fig. II.1).

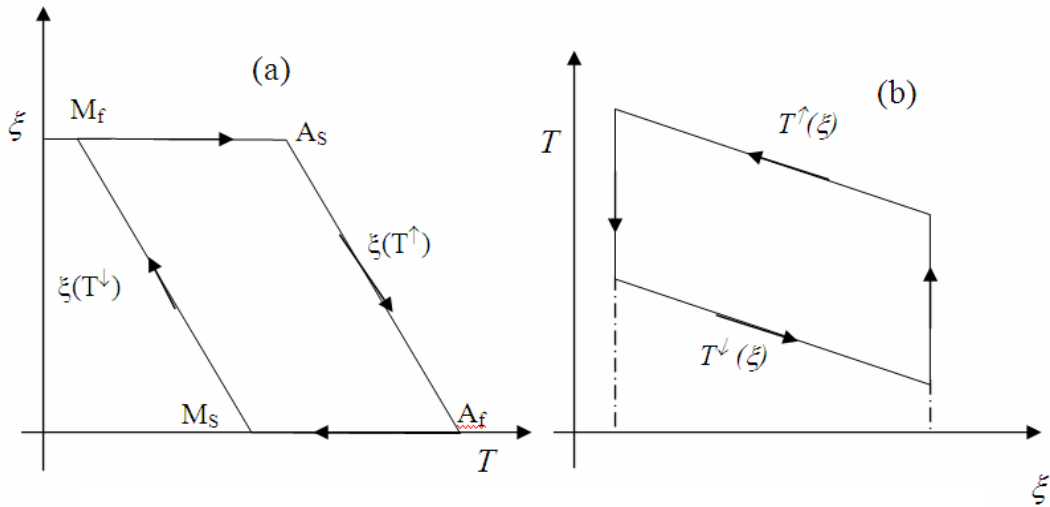


Fig. II.1. The $\xi(T^\downarrow)$ and $\xi(T^\uparrow)$ functions (a) and their inverses (b).

Fig. II.2. illustrates the shape of the hysteresis curves for the following schematic cases: a) both $d(\xi)$ and $e(\xi)$ are zero; b) $e(\xi)=0$ and $d(\xi)\neq 0$, but $d(\xi)$ is constant; c) $d(\xi)$ is constant and $e(\xi)$ linearly depends on ξ . It can be seen that in a) the transformation takes place at T_o , in b) there is already a hysteresis, but the $\xi(T^\downarrow)$ and $\xi(T^\uparrow)$ branches are vertical. In this case T_0 can be found as $T_0 = \frac{M_s + A_f}{2}$ as it can be seen from (II.8), in accordance with the Tong-Waynman relation [II.8]. For the case of c) the hysteresis curve is tilted, reflecting the ξ dependence of e , so the branches have slopes because of the contribution of the ξ dependent e to the phase transformation.

In general case, i.e. in the presence of other external fields, causing also phase transformations (like, uniaxial stress, σ , magnetic field ,B, or pressure, p), Δg_c^\downarrow has the form

$$\Delta g_c^\downarrow = \Delta u_c^\downarrow - T\Delta s^\downarrow - \sigma V \varepsilon^{tr\downarrow} + p\Delta V^{tr\downarrow} - B\Delta m^{tr\downarrow} \quad (\text{II.9})$$

where V is the (molar) volume, ε^{tr} is the transformation strain as well as Δm^{tr} and ΔV^{tr} are the change of magnetization and volume of phase transformation, respectively. Then, similarly to the definition of T_0 , one can also define the equilibrium transformation stress, σ_o , as

$$\sigma_o(0) = \frac{\Delta u_c^\downarrow}{V \varepsilon^{tr\downarrow}(T=0)} = \frac{\Delta u_c^\uparrow}{V \varepsilon^{tr\uparrow}(T=0)} \quad (\text{II.10})$$

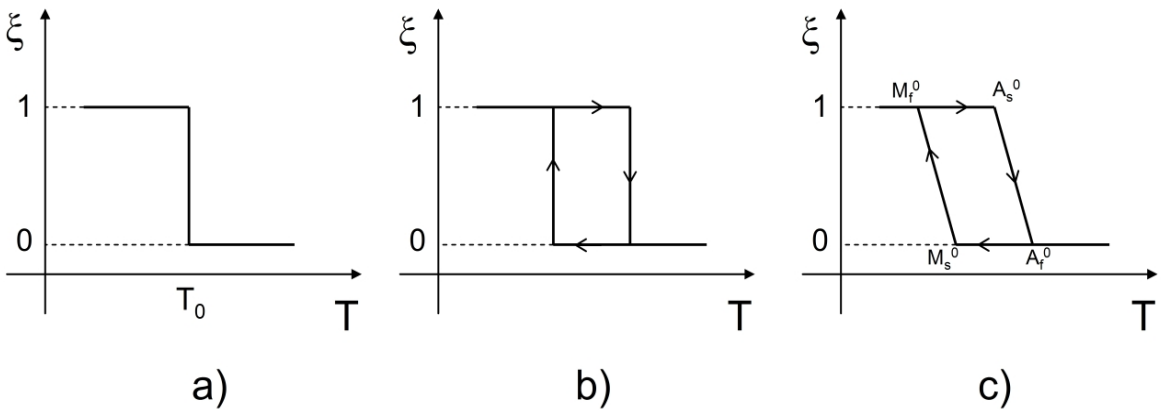


Fig. II.2. Martensite volume fraction (ξ) vs. temperature (T) considering the chemical (a) and non-chemical energy, (elastic (b) and dissipative (c)) contributions.

In the following the simultaneous effect of temperature and uniaxial stress is treated (extension to more general cases is very plausible). In this case T_0 (from $\Delta u_c^\downarrow - T\Delta s^\downarrow - \sigma V \varepsilon^{tr\downarrow} = 0$) has to be replaced by

$$T_0(\sigma) = T_0(0) + \frac{V \varepsilon^{tr\downarrow}(\sigma)}{-\Delta s}, \quad (\text{II.11})$$

giving the σ dependence of T_0 . Furthermore, instead of (II.10),

$$\sigma_0(T) = \frac{\sigma_0(0)\varepsilon^{tr}(\sigma_0)}{\varepsilon^{tr}(T)} - \frac{T \Delta s}{V \varepsilon^{tr}(T)} = \frac{[T_0(0) - T] \Delta s}{V \varepsilon^{tr}(T)} \quad (\text{II.12})$$

holds for the temperature dependence of σ_0 . It can be seen that (II.11) and (II.12) are the well known Clausius-Clapeyron relations and they are linear only if $\varepsilon^{tr}(\sigma)$ as well as $\varepsilon^{tr}(T)$ are constant.

In general the terms containing ε^{tr} (or Δm^{tr}) have tensor character and, even if one considers uniaxial loading condition, leading to scalar terms in (II.2), the field dependence of them is related to the change of the variant (magnetic domain) distribution in the martensite phase with increasing σ . Thus, at zero σ values thermally induced, randomly oriented multi-variant martensite structure (or multi-variant magnetic domain structure) forms in thermal hysteresis, while at high enough values of σ a well oriented array i.e. a single variant (or single domain) structure develops. Accordingly, ε^{tr} has maximal value for the single variant structure, while it can be close to zero for thermally induced multi-variant structure. Thus, ε^{tr} can depend on T or σ taking the $\xi(\sigma)$ or $\xi(T)$ hysteresis loops, respectively.

II.2.2 Mechanical hysteresis loop

Similarly as relations (II.6)-(II.8) were obtained, expressions for the branches of the $\xi(\sigma)$ or $\varepsilon(\sigma)$ (in measurements it can be usually assumed that $\varepsilon \sim \xi$) hysteresis loops (see Fig. II.3) are given by

$$\sigma^\downarrow(\zeta) = \sigma_0(T) + \frac{d(\zeta) + e(\zeta)}{V \varepsilon^{tr}(T)} \quad (\text{II.13a})$$

$$\sigma^\uparrow(\zeta) = \sigma_0(T) - \frac{d(\zeta) - e(\zeta)}{V \varepsilon^{tr}(T)}. \quad (\text{II.13b})$$

Thus

$$\sigma^\downarrow(\zeta) - \sigma^\uparrow(\zeta) = \frac{2d(\zeta)}{V \varepsilon^{tr}(T)} \quad (\text{II.14})$$

and

$$\sigma^\downarrow(\zeta) + \sigma^\uparrow(\zeta) = 2\sigma_0(T) + \frac{2e(\zeta)}{V \varepsilon^{tr}(T)}. \quad (\text{II.15})$$

The simple relations (II.6)-(II.8) and (II.13) - (II.15) allow the determination of the dissipative and elastic energy contributions as the function of ξ at different fixed values of σ as well as T from the thermal and stress induced hysteresis loops, respectively. Thus, even the σ and T dependence of E and D can be calculated by integrating the $e(\xi)$ and $d(\xi)$ functions between $\xi=0$ and $\xi=1$.

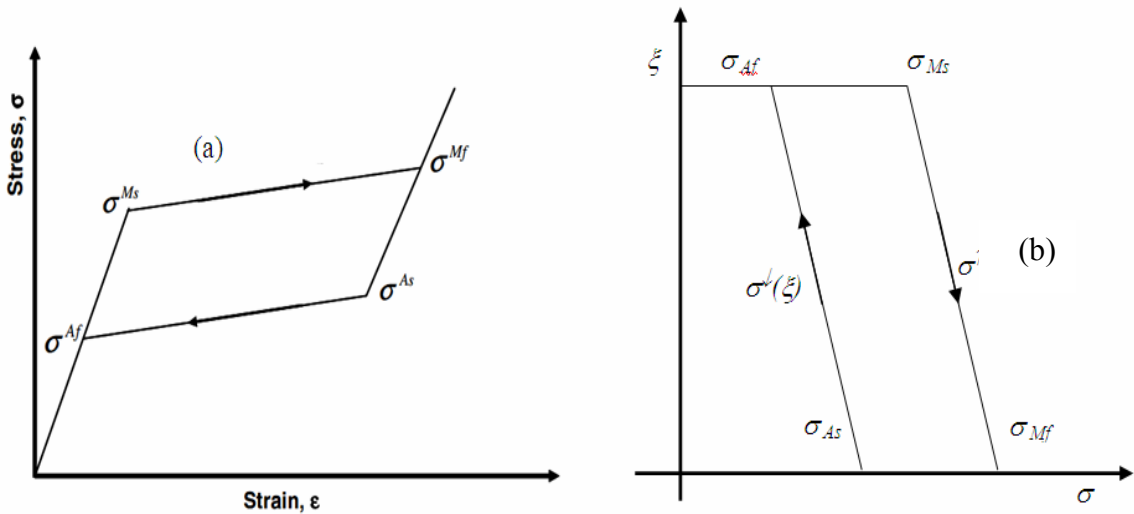


Fig. II.3. (a) Mechanical hysteresis loops and (b) their inverses.

The elastic energy contributions (see eqs. (II.8), (II.12) and (II.15)) can be determined only exclusive the term containing $T_o(0)$, if its value is not known. (The values of Δs can be obtained from DCS measurements (by integrating the dQ/T up and down curves, where Q is the heat of transformation: see also below) and the $\varepsilon^{tr}(T)$ and $\varepsilon^{tr}(\sigma)$ values can be read out from the $\varepsilon(\sigma)$ and $\varepsilon(T)$ hysteresis loops, respectively). Nevertheless, the stress and temperature dependence of the elastic energy contributions can be determined, since $T_o(0)$ appears only in the intercept of the $e(\sigma)$ and $e(T)$ or $E(\sigma)$ and $E(T)$ functions.

II.2.3 Start and finish temperatures and stresses

From relations (II.6) and (II.13) expressions for the start and finish temperatures as well as stresses can be simply obtained at $\xi=0$ and at $\xi=1$:

$$\begin{aligned}
 M_s(\sigma) &= T_o(\sigma) - \frac{d_0 + e_0}{-\Delta s} \\
 M_f(\sigma) &= T_o(\sigma) - \frac{d_1 + e_1}{-\Delta s} \\
 A_f(\sigma) &= T_o(\sigma) + \frac{d_0 - e_0}{-\Delta s} \\
 A_s(\sigma) &= T_o(\sigma) + \frac{d_1 - e_1}{-\Delta s}
 \end{aligned}
 \tag{II.16}$$

and

$$\begin{aligned}
 \sigma_{Ms}(T) &= \sigma_0(T) - \frac{d_0 + e_0}{-V \varepsilon^{tr}} \\
 \sigma_{Mf}(T) &= \sigma_0(T) - \frac{d_1 + e_1}{-V \varepsilon^{tr}} \\
 \sigma_{Af}(T) &= \sigma_0(T) + \frac{d_0 - e_0}{-V \varepsilon^{tr}} \\
 \sigma_{As}(T) &= \sigma_0(T) + \frac{d_1 - e_1}{-V \varepsilon^{tr}} .
 \end{aligned}
 \tag{II.17}$$

Here in principle the d_o , d_l , e_o and e_l can also be stress or temperature dependent: in this case e.g. the stress dependence of the start and finish temperatures can be different from the stress dependence of T_o . It can be seen from relations (II.16) that the simple expression proposed by Tong and Waynman [II.8] for T_o as $T_o = \frac{M_s + A_f}{2}$ can not be valid only if e_o is zero. Indeed, in their ingenious measurements Salzbrenner and Cohen [II.9] have been nicely illustrated that T_o can be calculated only in those cases when the elastic energy can be neglected as we mentioned above. In their paper the phase transformation was driven by a slowly moving temperature gradient in a single crystalline sample, which resulted in slow motion of only one interface across the specimen (single-interface transformation). This way the elastic energy could easily relax by the formation of the surface relief at the moving (single) phase-boundary. In general experiments for the determination of hysteresis loops this separation is not possible.

II.2.4 DCS measurements

It is worth summarizing what kind of information can be obtained from the analysis of the results obtained by a differential scanning calorimeter, DSC. The absorbed and released heat energies during the M/A and A/M transformations (see also Fig.II4.) can be given by

$$Q^\downarrow = \int [\Delta u_c^\downarrow + e(\xi) + d(\xi)] d\xi \quad (\text{II.18})$$

and

$$Q^\uparrow = \int [-\Delta u_c^\downarrow - e(\xi) + d(\xi)] d\xi. \quad (\text{II.19})$$

here $\Delta u_c^\downarrow = -\Delta u_c^\uparrow$ is the latent heat of transformation (per unit volume fraction).

It is worth noting that the heat measured is negative if the system evolves it: thus e.g. the first term in (II.18) has a correct sign, because it is negative ($\Delta u_c^\downarrow < 0$). Similarly the dissipative and elastic terms should be positive for cooling (the system absorbs these energies): indeed $e(\xi), d(\xi) > 0$, while for heating $e(\xi)^\downarrow = -e(\xi)^\uparrow = e(\xi)$ and $d(\xi)^\downarrow = d(\xi)^\uparrow = d(\xi)$.

Now, using the notations $\int \Delta u_c^\downarrow = \Delta U_c (< 0)$, $\int d(\xi)d\xi = D (> 0)$, $\int e(\xi)d\xi = E (> 0)$

$$Q^\downarrow = \Delta U_c + E + D \quad (\text{II.20})$$

and

$$Q^\uparrow = -\Delta U_c - E + D. \quad (\text{II.21})$$

(In obtaining (II.20) and (II.21) it was used that Δu_c^\downarrow is independent of ξ .)

Consequently

$$Q^\uparrow - Q^\downarrow = -2\Delta U_c + 2E \quad (\text{II.22})$$

and

$$Q^\uparrow + Q^\downarrow = 2D. \quad (\text{II.23})$$

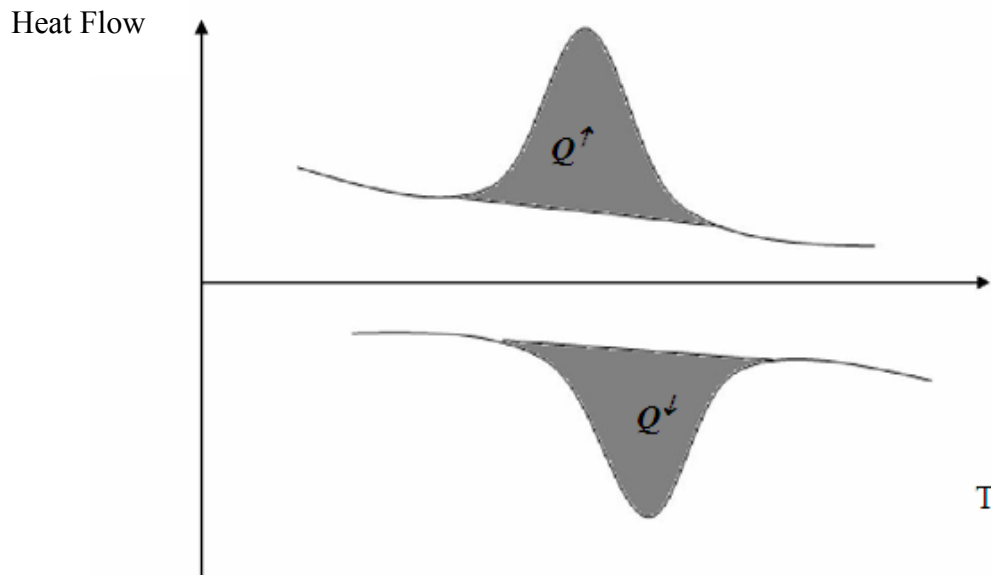


Fig. II.4. Schematic plot of DSC curve showing the gained Q^\uparrow and released Q^\downarrow heat.

It is important to keep in mind that the last equations are strictly valid only if after a cycle the system has come back to the same thermodynamic state, i.e. *it does not evolve from cycle to cycle*. Furthermore, it can be shown [II.14,II.15] that these are only valid if the heat capacities of the two phases are equal to each other: $C_A \cong C_M$.

The DSC curves also offer the determination of Δs . Indeed the integrals of the Q^\downarrow/T as well as Q^\uparrow/T curves between M_s and M_f , as well as between A_s and A_f , respectively give the Δs^\downarrow as well as Δs^\uparrow values. If, again the $c_A \cong c_M$ condition fulfils, then $\Delta s^\downarrow \cong -\Delta s^\uparrow$ [II.14,II.15].

Finally, it is possible, by using the DSC curve [II.7], to obtain the volume fraction of the martensite ξ as a function of temperature (both for cooling, T^\downarrow and heating T^\uparrow) as the ratio of the partial and full area of the DSC curve (A_{M_s-T} and $A_{M_s-M_f}$, respectively) (Fig. II.5.):

$$\xi \left(T^\downarrow \right) = \frac{A_{M_s-T}}{A_{M_s-M_f}} = \frac{\int_{M_s}^T \frac{dQ^\uparrow}{T}}{\int_{M_s}^{M_f} \frac{dQ^\uparrow}{T}} . \quad (\text{II.24})$$

Similar relation holds for the $\xi \left(T^\uparrow \right)$ curve (obviously in this case the above integrals run between A_s and T as well as A_s and A_f , respectively). The denominator is just the entropy of this transformation (see eq. (II.24)). Thus, the $e(\xi)$ and $d(\xi)$ energies can be calculated at $\sigma = 0$ according to relations (II.7 and II.8) .

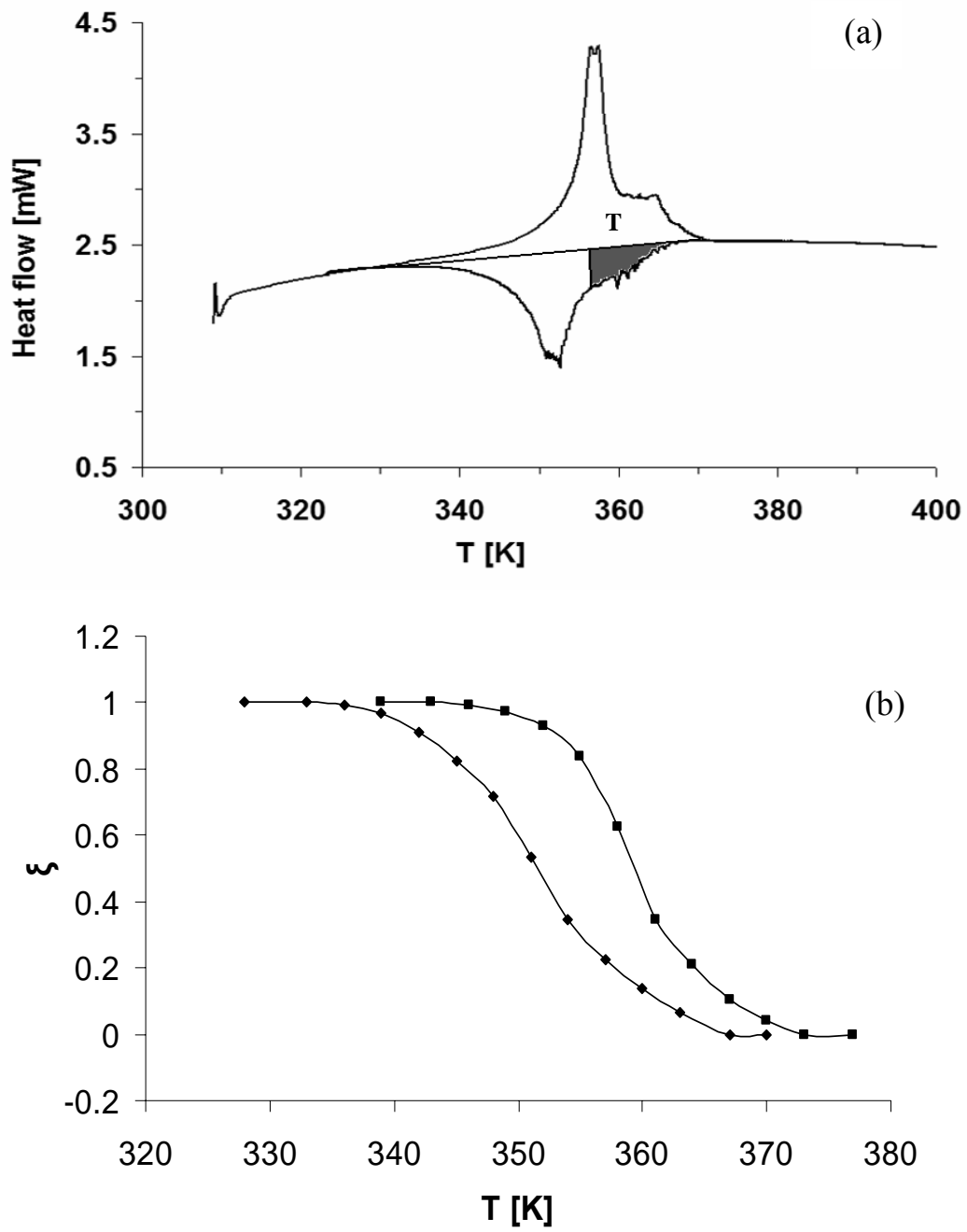


Fig. II.5. DSC curve measured at zero stress (a) and the $\xi(T)$ hysteresis curve (b) calculated from the DSC curve.

References

- [II.1] Z. Palánki, L. Daróczi, and D.L. Beke, *Mater. Trans.*, A46 (2005) 978.
- [II.2] L. Daróczi, D.L. Beke, C. Lexcellent and V. Mertinger, *Sripta Mat.*,43 (2000) 691.
- [II.3] Z. Palánki, L. Daróczi, C. Lexcellent and D.L. Beke, *Acta Mat.*, 55 (2007) 1823.
- [II.4] L. Daróczi, Z. Palánki, S. Szabó and D. L. Beke, *Material Sci. and Eng.*, A378 (2004) 274.
- [II.5] D.L. Beke, L. Daróczi, C. Lexcellent, V. Mertinger, *Journal de Physique IV* (France),115 (2004) 279.
- [II.6] D.L. Beke, L. Daróczi, Z.Palánki, *Proc. of Int. Conf. on Shape Memory and Superleastic Technologies*, 2007, Tsukuba, Japan, edited by S. Miyazaki (ASM International, Materials Park, Ohio) (2008) 607.
- [II.7] A. Planes, J.L. Macqueron , J. Ortin, *Phil. Mag. Let.*, 57 (6) (1988) 291.
- [II.8] H.C.Tong, C.M. Wayman, *Acta Metall.*, 22 (1974) 887.
- [II.9] R.J. Salzbrenner, M. Cohen, *Acta Metall.*, 27 (1979) 739.
- [II.10] D.A Porter, K.E. Easterling, “Phase Transformations in Metals and Alloys” Chapman and Hall, London, (1990).
- [II.11] H. Funakubo, “Shape Memory Alloys” Gordon and Breach, New York, (1986)
- [II.12] R. W. Cahn, and P.Hasen, (Eds.) “Physical Metallurgy” North Holland, Amsterdam, (1996).
- [II.13] J. Ortin, A. Planes, *Acta metal*, 36 (1989) 1873.
- [II.14] J. Ortin, A. Planes, *Journal de Physique*, IV, C4, Suppl., III/1 (1991) 13.
- [II.15] J. Ortin, A. Planes, *Acta metall.*, 36 (1988) 1878; 37 (1989) 1433.

Chapter III:

Experiments and Evaluation of Data

III.1 The samples

1. *Cu(79.2wt%)Al(15.9wt%)Ni(4.9wt%) single crystalline samples.* The samples were obtained from Prof. Jan Van Humbeeck (KUL Leuven, Belgium). Rods were cut by a simple spar erosion machine and the final dimensions were: 41 mm in length and 0.45 mm² in square cross section for elongation-temperature tests and 0.59 mm² for strain-stress tests. The stress was applied parallel to the [110]_A axis.
2. *Cu(88.04wt%)Al(11,6wt%)Be(0.36wt%) polycrystalline SMA samples* provided by Nimesis technology (Metz, France). The dimensions of the samples were 0.8 mm in diameter and 85mm in length.

III.2 Experimental techniques

III.2 .1 The stress-strain set-up

The stress-strain curves were obtained by a tensile machine (Chatillon TCD225; see Fig. III.1.) applying an external heating chamber using thermal resistance with temperature regulator for controlling the heating and cooling rate. The heating as well as cooling rates were 8K/min. The stress-induced hysteresis loops were determined between 373K and 423 K (at 8 fix temperatures).

III.2.2 Temperature–strain set-up

We developed our own machines for the determination of temperature-strain, T - ε , and temperature-resistance, T - R , curves at fixed loads (Fig.III.2.).

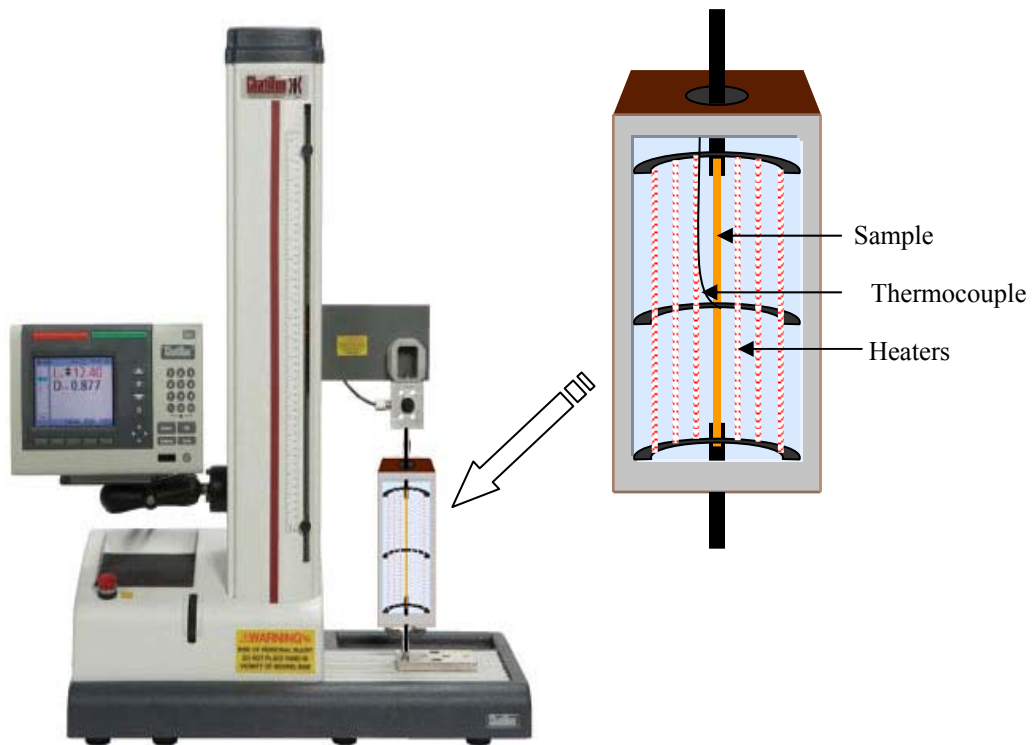


Fig. III.1. The tensile machine (Chatillon TCD225). The inset is the external heating system.

This developed system allows us to measure the resistance as well as the elongation of the samples by using the four wire method and by using a digital micrometer, respectively. A small resistance furnace is used to heat up the sample. To avoid the oxidation and the condensation of water vapor, the sample was placed in tube filled with H_2 and then put the system in liquid nitrogen for cooling down. The furnace is connected to a temperature regulator to keep the heating and cooling rate constant.

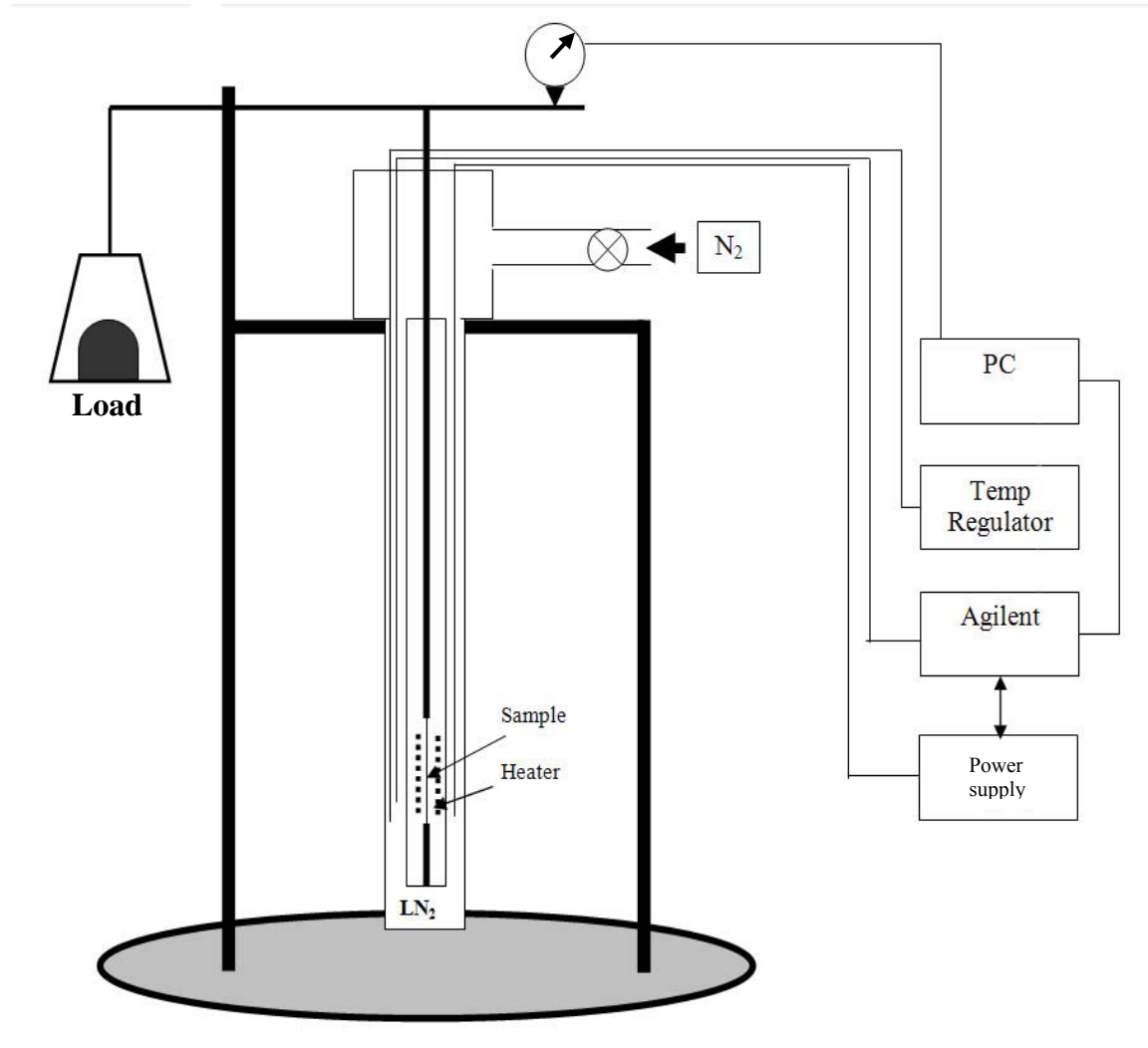


Fig. III.2. Scheme of the set-up for the determination of T- ϵ and T-R curves under fixed uniaxial stress.

III.2.3 DSC measurements

Perkin-Elmer DSC-7 power compensation differential scanning calorimeter (DSC) was used at zero uniaxial stress to measure the absorbed and the released heat during the martensitic transformation at different heating-cooling rates, as well as to make thermal cycling on the samples.

The entropy of transformation was estimated from the obtained curves, according to the relation

$$\Delta s = \Delta s^\downarrow = \int_{M_s}^{M_f} \frac{dQ^\downarrow}{T} \cong -\Delta s^\uparrow = \int_{A_s}^{A_f} \frac{dQ^\uparrow}{T}. \quad (\text{III.1})$$

Here Q^\uparrow and Q^\downarrow denote the absorbed and released heat during the up and down transformations, respectively. Note that (III.1) is valid only if the heat capacity of the austenite and martensite phases are the same [III.1, III.6]. Since the difference of the magnitudes of the entropy changes, estimated from the up and down curves, were the same within the experimental error, this approximation was used.

There are many parameters controlling the thermoelastic transformation: the chemical composition, temperature, applied stress and its orientation relative to the single crystal axis [III.2-III.5]. In the investigated temperature and stress range only the transformation from the high temperature cubic β phase to the β' (18R) phase takes place [III.2, III.3] in single crystalline samples. In the polycrystalline CuAlBe samples the same type of phase transformation takes place [III.7].

III.3 Experimental results

All results presented in this chapter were published in [III.8] and [III.10].

III.3.1 Single crystalline samples

III.3.1.1 DSC Measurements

Figure III.3. shows the DSC curves measured. Both the heating and cooling rate were 2K/min. According to the relation (III.1), the absolute values of the entropy were calculated from the heating and cooling branches. The two values were nearly the same (the difference was within the experimental errors) $\Delta s = -1.26$ J/Kmol. This value is in good agreement with the values obtained in alloys of similar composition and having β phase to β' phase transformation [III.3]. The molar volume of our sample was $V = 7.9 \cdot 10^{-6}$ m³/mol.

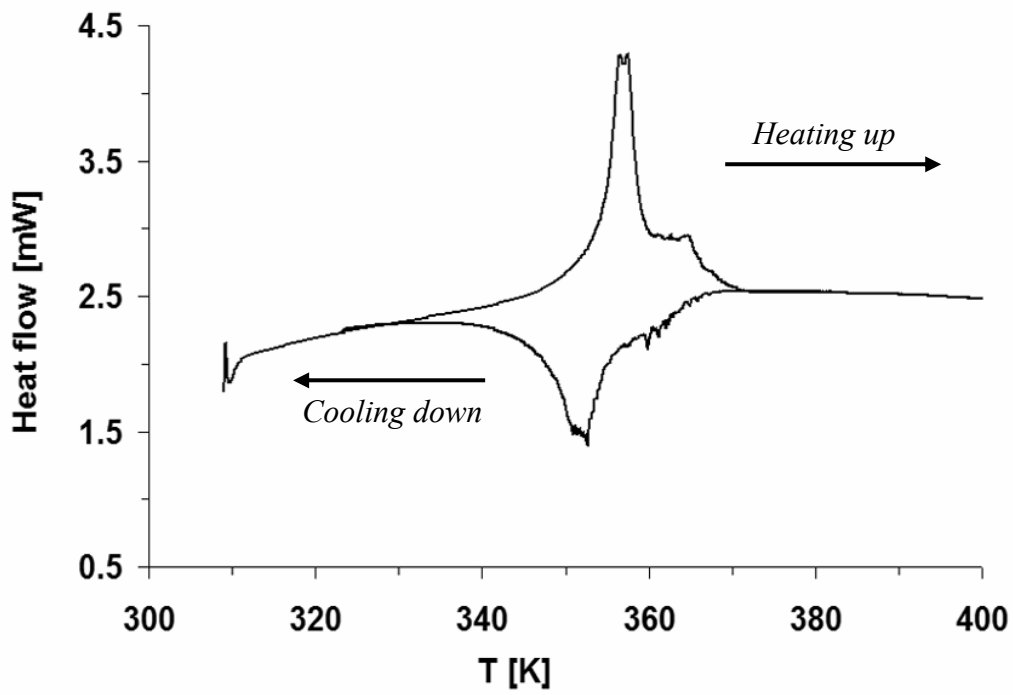


Fig. III.3. DSC curve measured at zero stress.

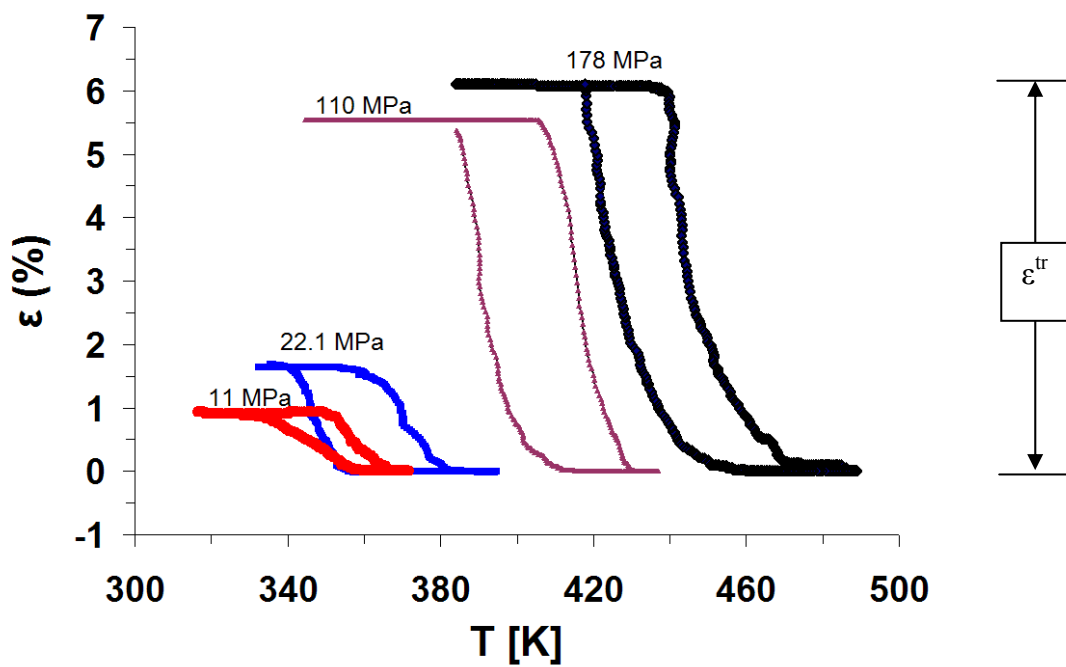


Fig. III.4. Thermal hysteresis loops (ϵ vs. T curves) at four different uniaxial stress levels.

III.3.1.2 Thermal Hysteresis loops (ε -T loops)

Fig. III.4. shows the strain-temperature hysteresis loops at different constant uniaxial stress levels. It can be seen that at lower stress levels, the transformation strain, ε^{tr} , is small and there is a sudden increase between 15 and 30 MPa. Using Fig.III.4. the transformation strain as a function of the applied stress can be calculated as shown in Fig. III.5. illustrating that there is a saturation of the ε^{tr} value after 40 MP: this saturation value is about 6 %.

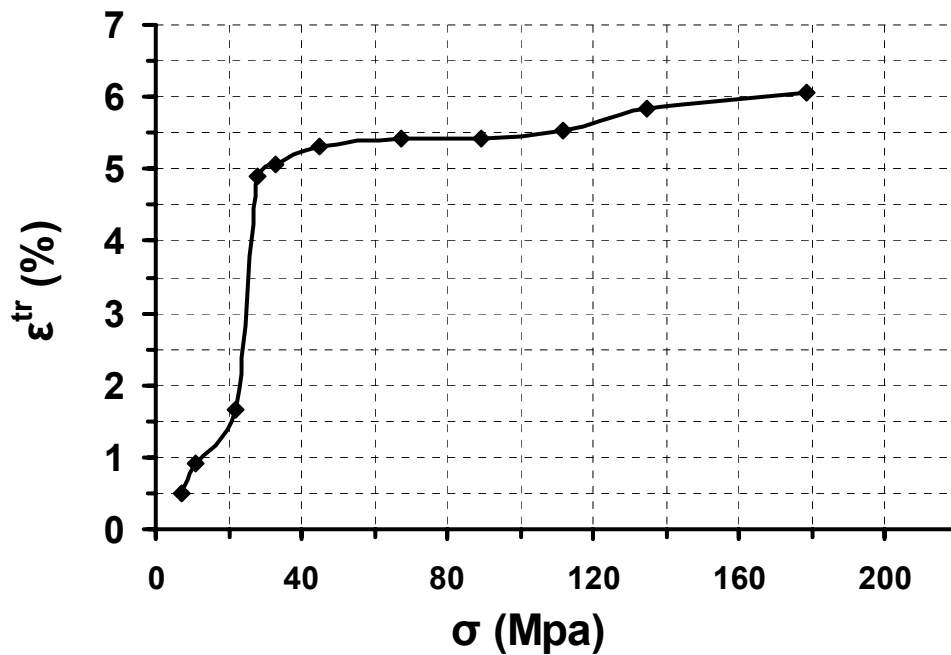


Fig. III.5. Transformation strain as a function of stress (ε^{tr} is the maximal of value of ε in Fig. III.4.).

III.3.1.3 Strain-stress hysteresis loops

Strain-stress (ε - σ) hysteresis loops measured at different constant temperatures are shown in Figure III.6. All curves were obtained at temperatures greater than A_f . We can see that all curves turn back to the starting points (i.e. to $\varepsilon=0$) showing *pseudo elastic* behavior. Fig. III.7. shows the transformation strains as a function of temperature: they were calculated from the $\sigma(\varepsilon)$ loops (see Fig. III.6.). It can be seen that there is a large change between 355 and 383 K before reaching the saturation: the

saturation value of the transformation strain is about 6 %, similar to the value shown on Fig. III.5.

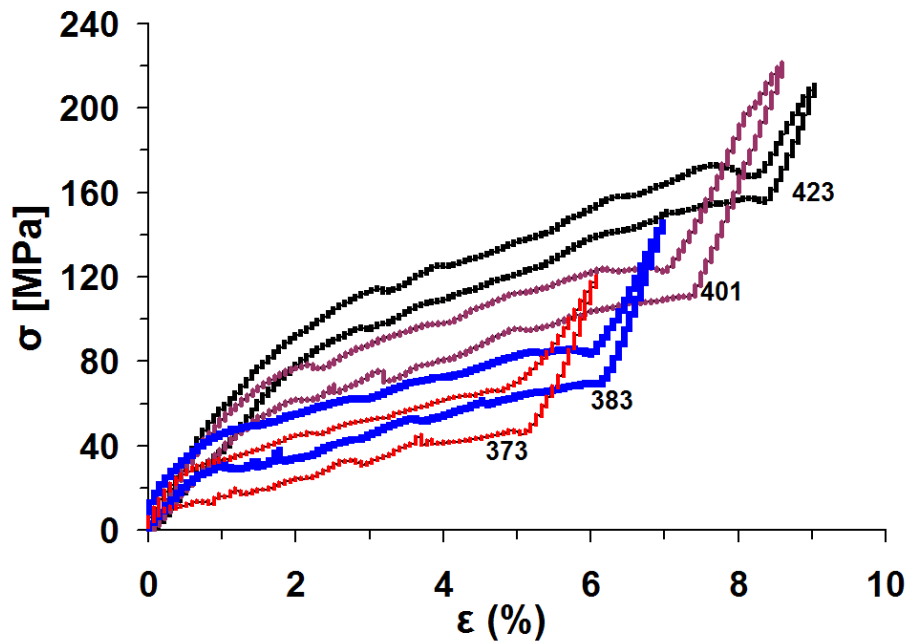


Fig. III.6. σ versus ϵ at four different temperatures.

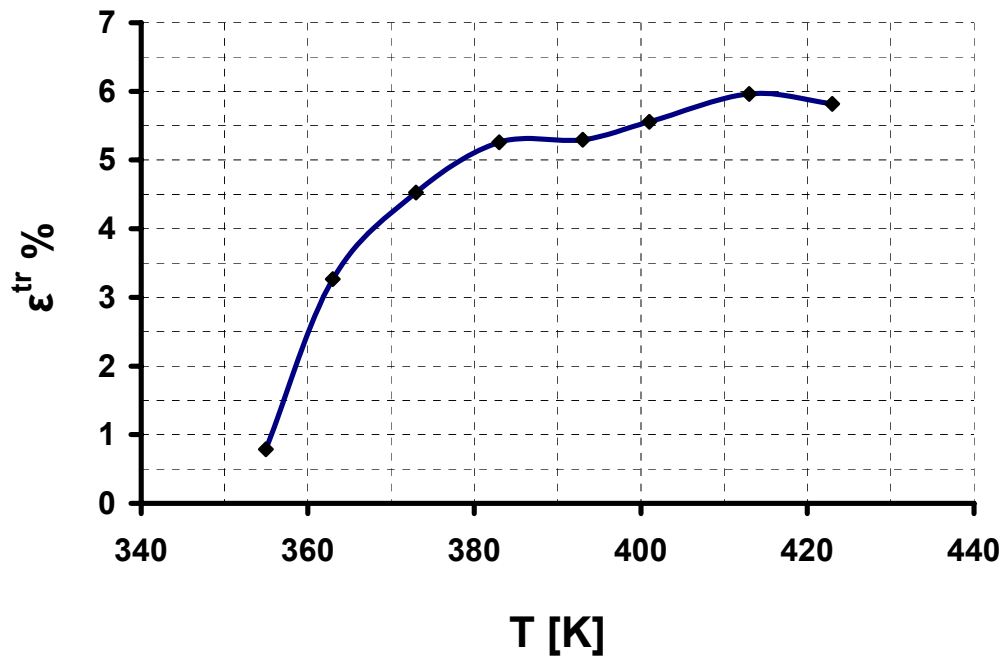


Fig. III.7. Transformation strain as a function of temperature (read out from curves shown in Fig. III.6.).

III.3.1.4 Temperature and stress dependence of the start and finish stresses and temperatures

From Fig. III.4. and from Fig. III.6. one can determine the transformation temperatures M_S , A_S , M_f and A_f as well as the transformation stresses σ_{M_S} , σ_{A_S} , σ_{M_f} and σ_{A_f} . The procedure is shown in Fig. III.8. where the ideal form of *the* $\varepsilon(T)$ hysteresis curve is shown.

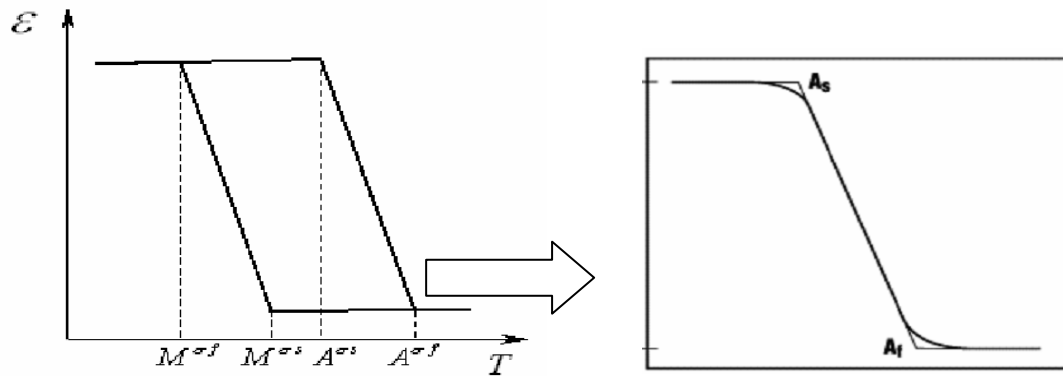


Fig. III.8. Determination of M_S , A_S , M_f and A_f temperatures from the $\varepsilon \sim T$ curves.

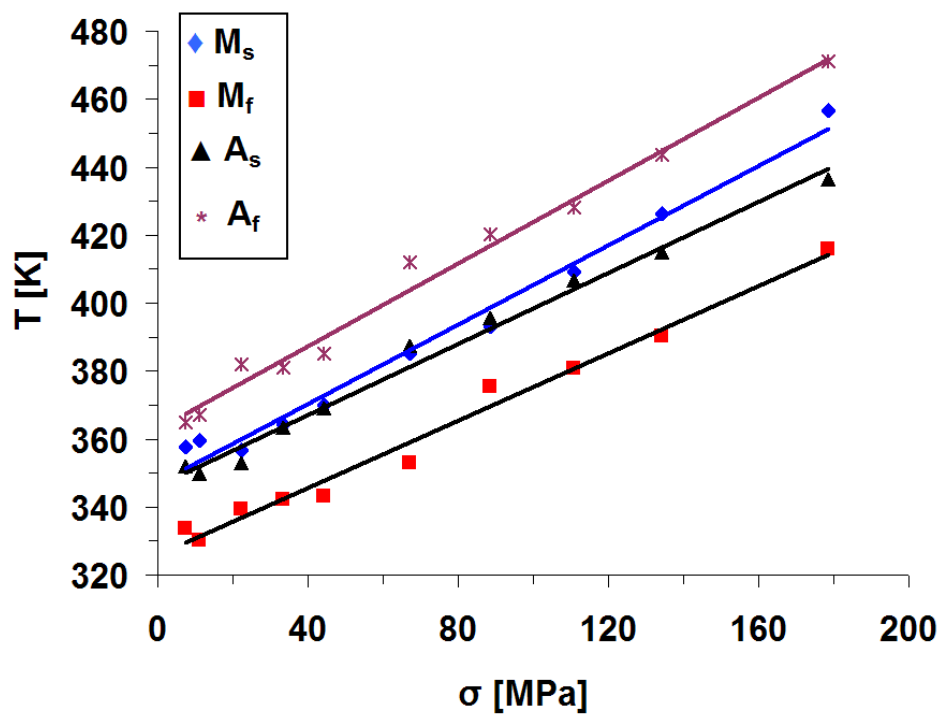


Fig. III.9. Start and finish temperatures as the function of stress.

Figs. III.9. and III.10. show the stress and the temperature dependence of the start and finish temperatures and stresses, respectively. One can see that the transformation temperatures and transformation stresses strongly depend on the applied stress and temperature, respectively. The slopes of transformation temperatures as well as transformation stresses are given in Table III.1.

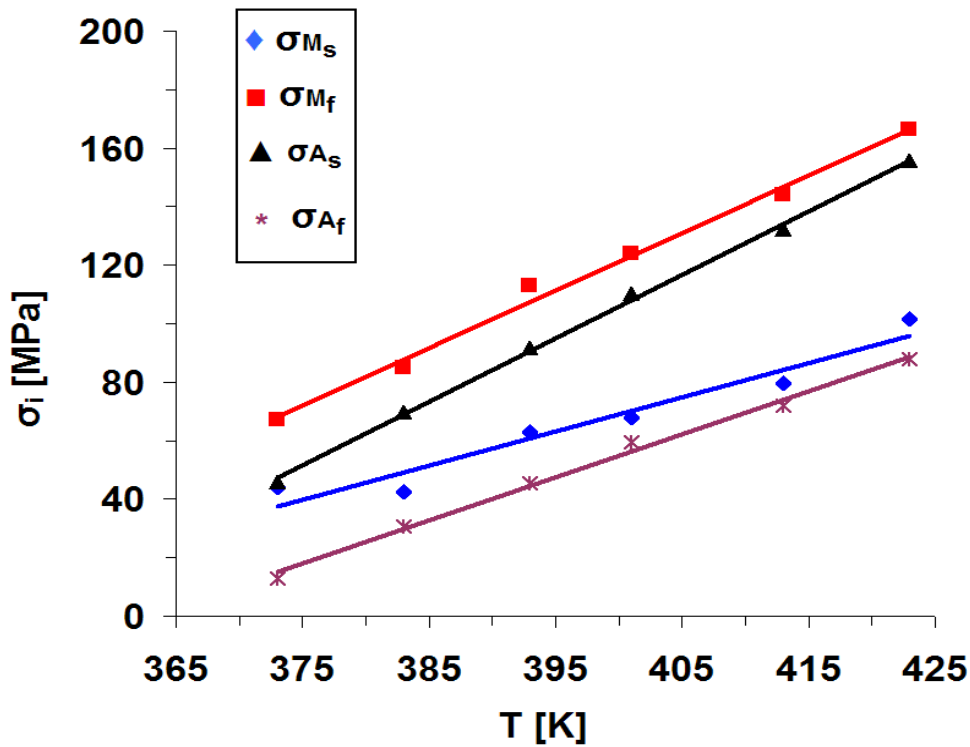


Fig. III.10. Start and finish stresses as the function of temperature.

	SLOPE (K/MPA)		SLOPE (MPA/K)
M_s	0.58	σ_{M_s}	1.60
M_f	0.5	σ_{M_f}	1.96
A_s	0.52	σ_{A_s}	2.17
A_f	0.61	σ_{A_f}	1.54

Table III.1. The slopes calculated from the curves shown in Fig.III.9. and Fig.III.10.

III.3.1.5 Cycling effect

Deeper understanding of the thermomechanical cycling effects on the transformation can lead to improved control of the shape memory function. Many applications of shape memory devices e.g. actuators require a large number of thermal and mechanical cycles and also a stable and reliable shape memory effect. Training or teaching the *SMA* refers to applying an external field such as thermal or mechanical loading cycles until the stabilization of all the *SMA* parameters e.g. start and finish temperatures as well as start and finish stresses [III.9]. As a first step to understand the basic mechanisms of fatigue we carried out investigations on the effect of number of thermal and stress driven cycling on the β to β' phase transformation in single crystalline CuAl(11.5wt%)Ni(5.0wt%) alloy [III.10].

III.3.1.5.1 Thermal cycling

Thermal cycling was carried out by using a differential scanning calorimeter, DSC, at zero uniaxial stress and 10 K/min heating and cooling rate. The transformed martensite fraction, versus temperature curves as well as the heat of transformations, Q , at zero stress was obtained. Fig. III.11. shows the DSC heating and cooling curves obtained at zero stress. Fig. III.12. shows the normalized ε - T hysteresis loops calculated from the DSC curves for three different N. It can be seen that both the area of the loops and the slopes of the upper and lower branches have systematic changes with N.

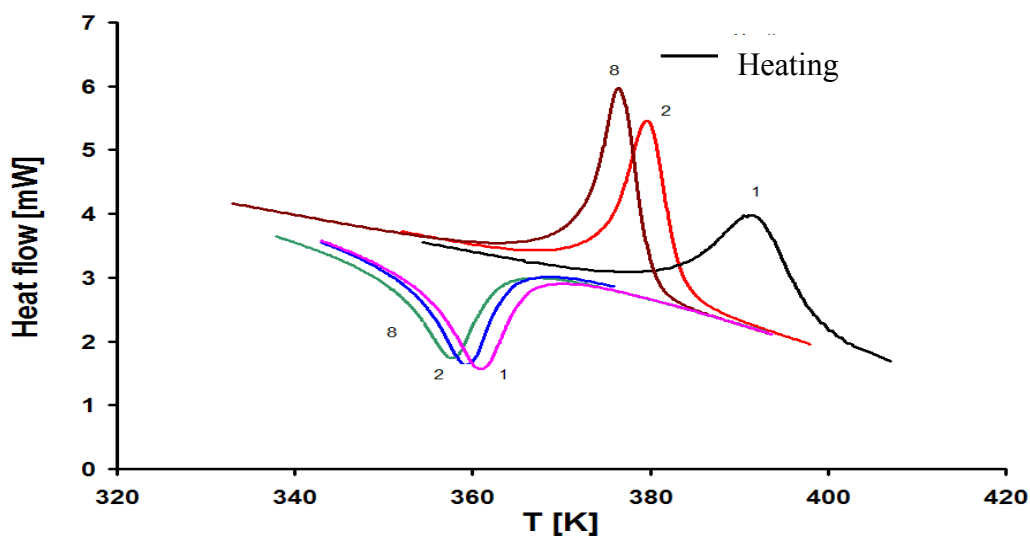


Fig. III.11. DSC curves at zero stress for different cycles.

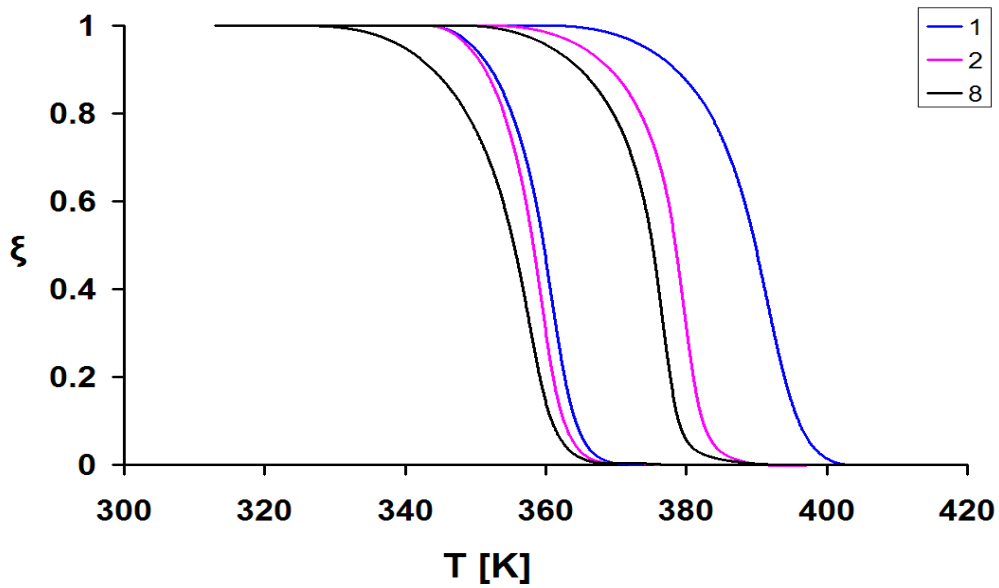


Fig. III.12. Hysteresis loops calculated from the DSC curves.

III.3.1.5.2 Mechanical cycling

Mechanical cycling was carried out to see the effect of the cycling on the dissipative and elastic energies. The stress-strain curves for different cycles, at 373 K (starting from the austenite phase, $T > A_s$) are shown in Fig. III.13. As one can see there is a moderate increase in the transformation strain at higher number of cycles.

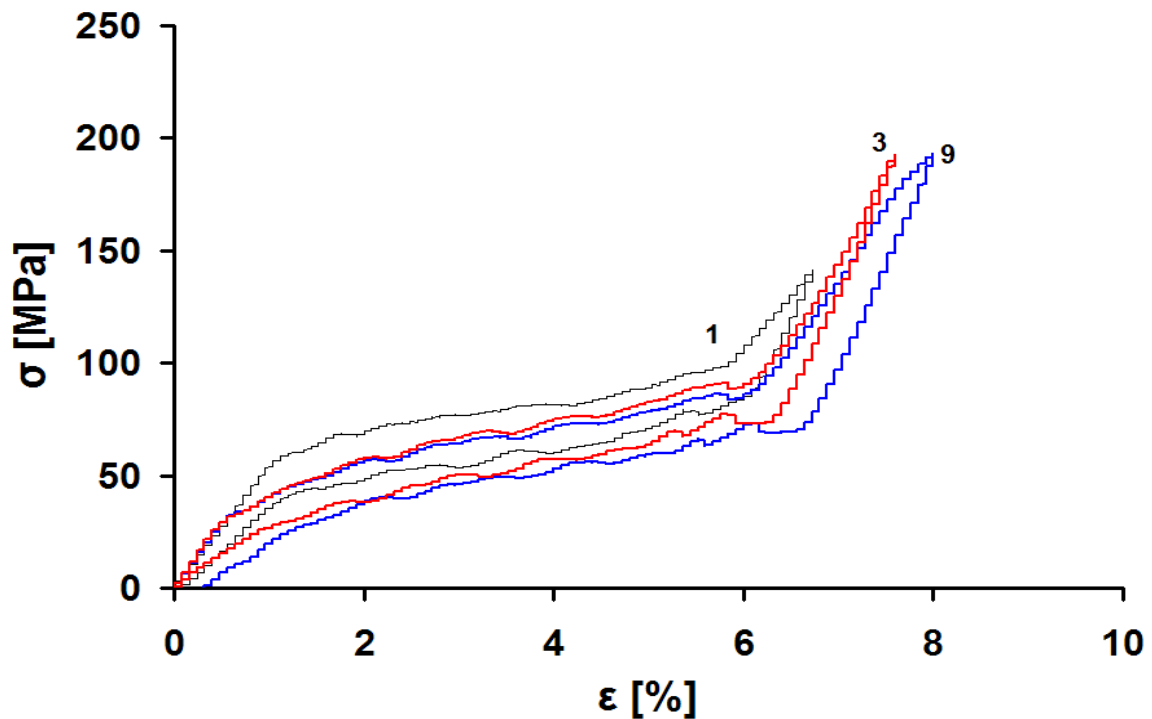


Fig. III.13. σ versus ϵ at different number of cycles at fixed temperature.

III.3.2 Polycrystalline samples

We have seen before that at higher stresses the elastic energy decrease, so we investigated the effect of the high stress on the dissipative and the elastic energies in the CuAl(11,6wt%)Be(0.36wt%) polycrystalline shape memory alloy too. The resistance – temperature (R - T) hysteric loops at constant stresses are shown in Fig. III.14. The normalized curves coming from the R - T hysteric loops are shown in Fig. III.15. One can see that the loops shift to higher temperatures at higher stress, and the slopes of the branches increase indicating a lower elastic energy contribution.

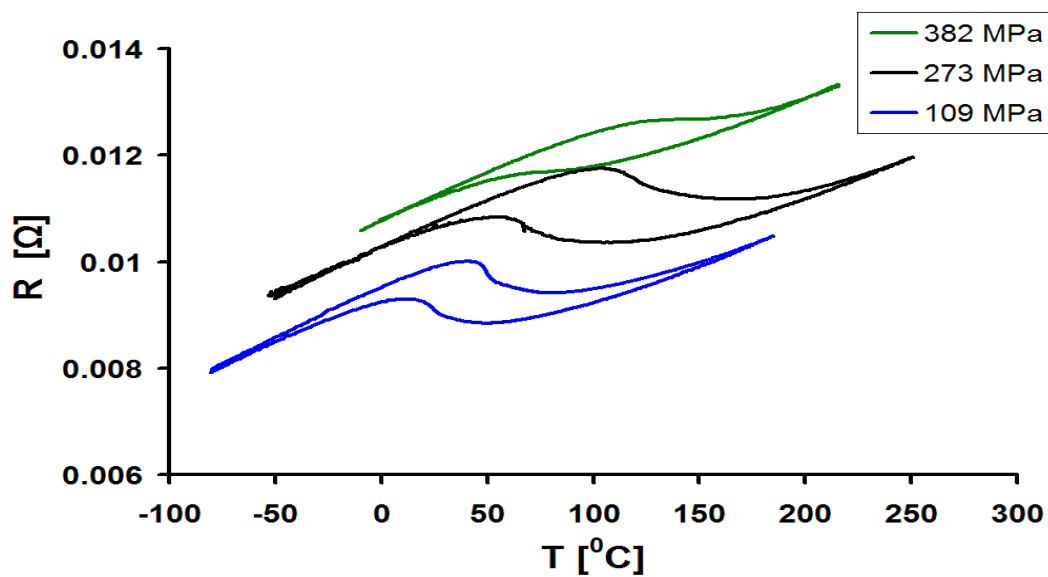


Fig. III.14. Stress dependence of the R - T with hysteresis loops.

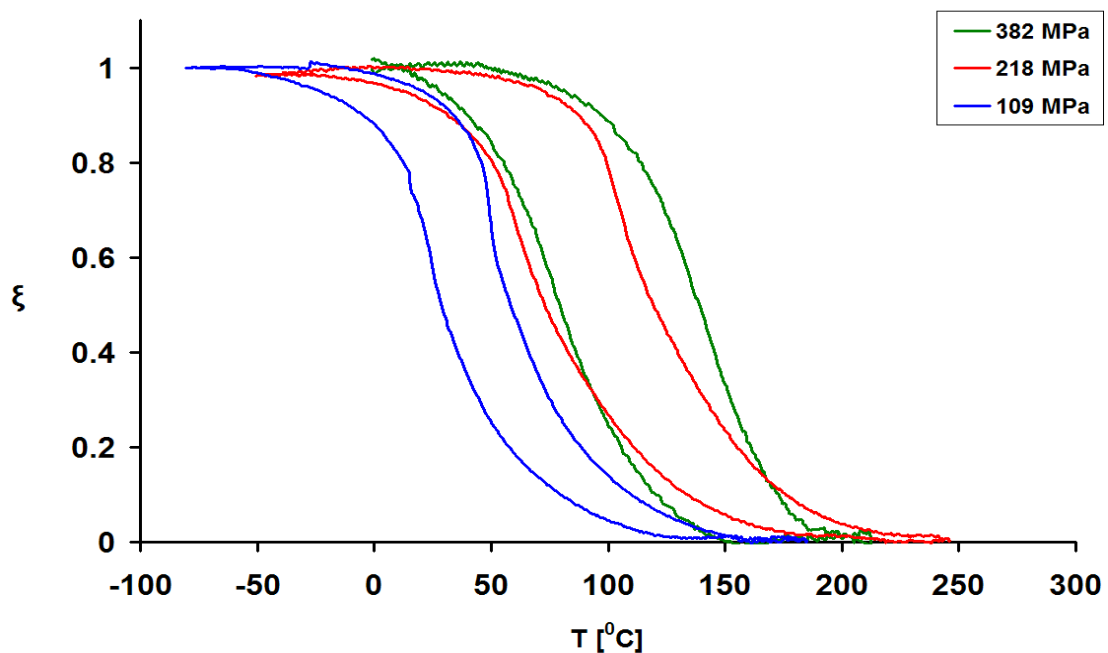


Fig. III.15. Normalized R - T curves.

References

- [III.1] J. Ortín and A. Planes: Thermodynamic analysis of thermal measurements in thermoelastic martensitic transformation, *Acta Metallurgica*, 36/8 (1988) 1873.
- [III.2] V. Recarte, R.B. Perez-Seaz, E.H. Bocanegra, M.L. No. *J. San Huan, Mat. Sci. Eng.*, A273-275 (1999) 380.
- [III.3] V. Recarte, J.I. Perez-Landazabal, P.P. Rodriguez, E.H. Bocanegra, M.L. No. *J. San Huan, Acta Mater.*, 52 (2004) 3941.
- [III.4] V. Novak, J. Malimanek, N. Zarubiva, *Mat. Sci. Eng.*, A191 (1995) 193.
- [III.5] R. Gastien, C.E. Corbellani, H.H. Alvarez Villar, M. Sade, F.C. Lovey, *Mat. Sci. Eng.*, A349 (2003) 191.
- [III.6] T.W. Duerig, K.N. Melton, D. Stockel, C.M. Wayman (Ed), "Engineering aspects of shape memory alloys" (London: Butterworth-Heinemann) (1990).
- [III.7] S. Montecinos, A. Cuniberti, *J. of Alloys & Comp.*, 457 (2008) 332.
- [III.8] T.Y. El Rasasi, L. Daróczy, D.L. Beke, *Intermetallics*, 18 (2010) 1137.
- [III.9] Dimitris C. Lagoudas (Ed), "Shape Memory Alloys" Springer Science+Business Media, LLC (2008).
- [III.10] T.Y. El Rasasi, L. Daróczy, D.L. Beke, in print in *J. of Alloys and Compounds*.

Chapter IV

Analysis of Experimental Data

IV. 1 Result on single crystalline samples

IV.1.1 Temperature and stress dependence of the transformation strain

Let us consider now the $\varepsilon^r(\sigma)$ and $\varepsilon^r(T)$ functions obtained from $\varepsilon \sim T$ and $\varepsilon \sim \sigma$ hysteresis loops and illustrated in Figs. III.5. and III.7. It can be seen that both $\varepsilon^r(\sigma)$ and $\varepsilon^r(T)$ has a sudden change between 15 and 30 MPa as well as 355 and 483 K respectively. The saturation values for both of them are the same, about 6%. The field dependence of ε^r is related to the change of the martensite variant distribution with increasing field parameters [IV.1]. Indeed, ε^r can be very small or even close to zero for the formation of the thermally induced (randomly oriented) martensite variants (usually there is a very small resultant (remnant) strain in single crystalline samples, as seen in Fig III.5.).

For the description of this, the volume fraction of the stress-induced (single) variant martensite structure, η , has been introduced in [IV.1]. Accordingly, the stress as well as the temperature dependence of ε^r can be expressed via the η dependence of $\varepsilon^r(\eta)$ as

$$\varepsilon^r = \varepsilon_T + (\varepsilon_\sigma - \varepsilon_T) \eta, \quad (\text{IV.1})$$

where ε_T and ε_σ are the transformation strains when fully thermally induced multi variant structure forms ($\eta=0$), as well as when the martensite consists of a fully ordered array of stress preferred variants (single variant state, $\eta=1$), respectively.

It is worth noting that in Fig. III.6. the martensite start stress at 373 K is about 30 MPa and on the curve shown in Fig. III.5. this leads to about 4% ε^r value, which is approximately the same as was observed at this temperature (see Fig. III.7.). Since in the expression for Δg ($\Delta g = \Delta u - T\Delta s - \sigma V \varepsilon^r$), the elastic and thermal terms play

equivalent roles with opposite sign in the thermoelastic balance [IV.2, IV.3], at higher temperatures higher stress is necessary to start the transformation and the formed martensite structure will be more oriented: η and thus ε^r will be larger.

IV.1.2 Analysis of the results on thermal hysteresis loops

In the relations presented in the section II.2, we can see that $T_o(\sigma)$ is not linear in general because of the transformation strain $\varepsilon^r(\sigma, T)$ is not constant (see Fig. III.5.), furthermore, the elastic and dissipative terms ($e_i, d_i, i=0,1$) as a function of the stress can also contribute the stress dependence of the start and finish temperatures (see relations (II.16)). Thus, we plotted the $T_o(\sigma)-T_o(0)$ values versus σ in Fig. IV.1. using the relation (II.11) and the measured value of $\Delta s/V$ and the $\varepsilon^r(\sigma)$ curve (Fig. III.5.). By neglecting the small deviations in the interval between 0 and 40 MPa in Fig IV.1. we can see that this function can be approximated by a straight line. This small deviation - S-shape part up to 40MPa - is coming from the stress dependence of ε^r (see the inset in Fig. IV.1.). The slope of the fitted straight line in the whole stress range is 0.39 ± 0.05 K/MPa, and from Table III.1. the slopes of M_s and A_f as well as M_f and A_s (see Fig. III.9. and Table III.1.) are practically the same: 0.59 as well as 0.50 K/MPa, respectively. Thus, these slopes are different from the obtained slope of the $T_o(\sigma)$.

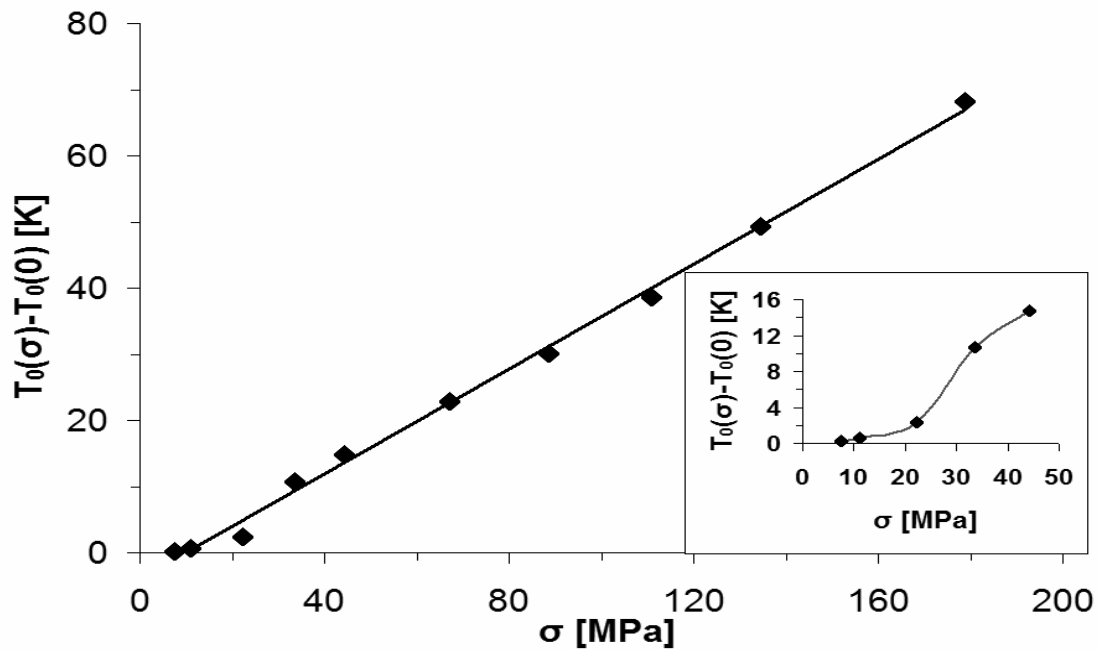


Fig. IV.1. Calculated stress dependence of the equilibrium transformation temperature, T_o .

We can study the effect of the contribution of the stress dependence of d_i and e_i parameters in the difference slopes. We can calculate d_0 and d_1 by using the relation (II.16) by taking the difference of the $A_f(\sigma)$ and $M_s(\sigma)$ and $A_s(\sigma)$ and $M_f(\sigma)$, respectively. As well as the e_o and e_l in terms of $T_o(0)\Delta s$ can be calculated from the sums of the $M_s(\sigma)+A_f(\sigma)$ and $M_f(\sigma)+A_s(\sigma)$, respectively with the help of the quantities $\sigma V \varepsilon''(\sigma)$.

Fig. IV.2. shows the stress dependence of the d_o and d_l quantities. It can be seen that, there is an increase up to 60 MPa then decrease again for both d_0 and d_l : the maximum is around 18 and 22 J/mol for d_0 and d_l respectively. It is worth mentioning that the maximum value is around the point corresponding to the where stress value of the saturation of $\varepsilon''(\sigma)$ starts. This can be related to the change in the formation of thermally induced (randomly oriented) and stress-induced (well oriented) martensite variants. ***At lower stresses many different variants with high dissipation are present, but by increasing the applied uniaxial stress, one variant will be preferred and hence the dissipation will be a bit lowered.***

But even if we take the average value of d_i ($i=1$ or 0) and consider its error, the average value is about 12 ± 3 J/mol for both d_0 and d_l . However, it is clear that the deviation reflected in the different slopes of T_0 as well as of the start and finish temperatures originate not from the dissipative contributions.

On the other hand, we can see that from Fig. IV.3. that the e_o and e_l parameters have a linear stress dependence. The vertical axis of this figure is $T_o(0)\Delta s + e_i$ ($i=0,1$). Note that since the $T_o(0)\Delta s$ quantity is negative ($\Delta s < 0$) and, thus from the fact that the values on the vertical axis are negative, one can conclude that $e_o(0) < |T_o(0)\Delta s|$.

The slopes of these curves are - 0.25 and - 0.14 J/molMPa, respectively, or dividing them by Δs we have the contributions of the elastic energy contributions to the slopes of the start and finish temperatures (see eq. (II.17)): $\partial(e_o/\Delta s)/\partial\sigma = 0.20$ K/MPa and $\partial(e_l/\Delta s)/\partial\sigma = 0.11$ K/MPa, respectively. Taking into account that the errors in the estimation of slopes are about ± 0.05 K/MPa, it can be concluded that the difference between the slopes of the $T_o(\sigma)$ and $M_s(\sigma)$ or $A_s(\sigma)$ is caused by the stress dependence of the elastic energy contributions [IV.4].

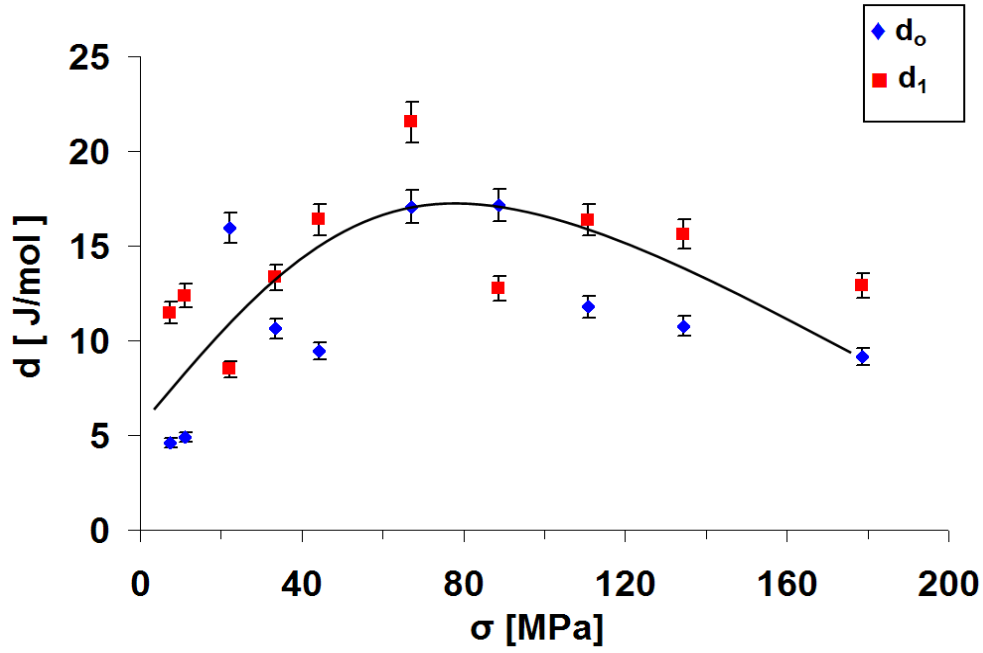


Fig. IV. 2. Stress dependence of the dissipative terms.

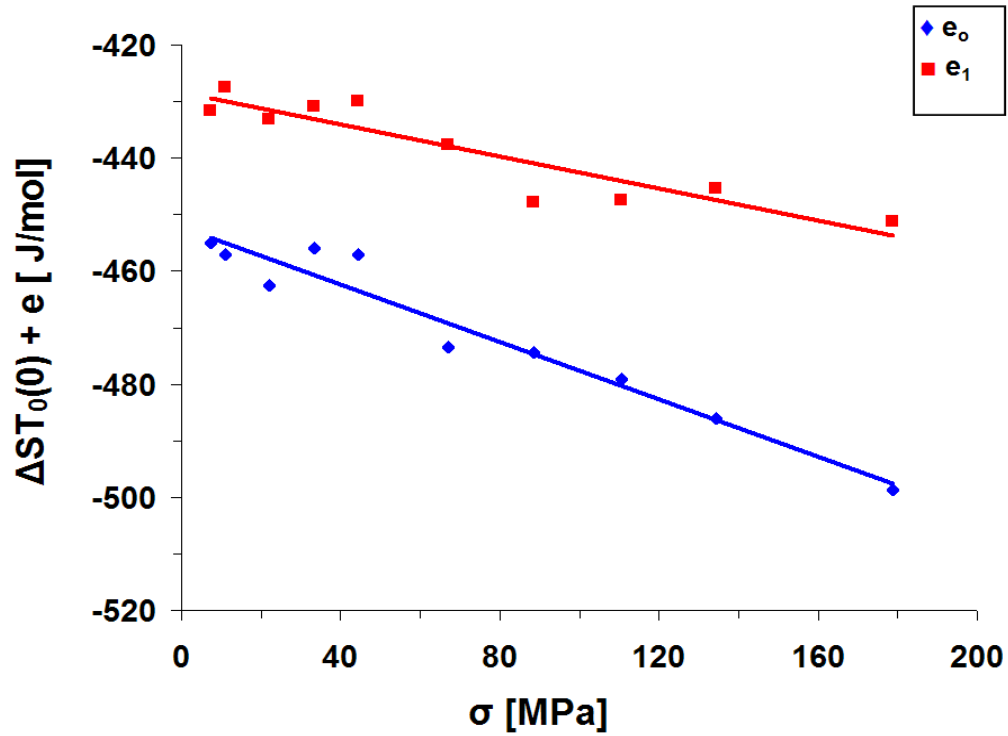


Fig. IV.3. Stress dependence of the elastic energy terms.

IV.1.3 Analysis of the results obtained from σ - ε hysteresis loops

The determination of the temperature dependence of $\sigma_o(T)$ is difficult because we can not apply a similar procedure as for the stress dependence of $T_o(\sigma)$, because

we do not know the value of $T_o(0)$ (see eq. (II.12)), where ε^{tr} has temperature dependence as seen in Fig. III.7.). Nevertheless, the slopes of the straight lines fitted to the start and finish stresses versus temperature functions (Fig. III.10) are given in Table III.1. Furthermore, the $d_i(T)$ and $e_i(T)$ functions, are shown in Figs. IV.4. as well as IV.5., respectively as calculated from the differences of $\sigma_{Af}(T)$ and $\sigma_{Ms}(T)$ and the sums of the $\sigma_{As}(T)$ and $\sigma_{Mf}(T)$ curves (see Fig. III.10 and Table III.1.), and using the $\varepsilon^{tr}(T)$ values given in Fig. III.7. For the elastic terms one can write, by using relations (II.10), (II.12) and (II.17),

$$\begin{aligned} \frac{V \varepsilon^{tr}(T) [\sigma_{Ms}(T) + \sigma_{Af}(T)]}{2} + T \Delta s &= V \varepsilon^{tr}(T) \sigma_0(T) + e_0(T) \\ &= T_o(0) \Delta s + e_0(T) \\ &= \sigma_0(0) V \varepsilon_o^{tr} + e_0(T). \end{aligned} \quad (IV.2)$$

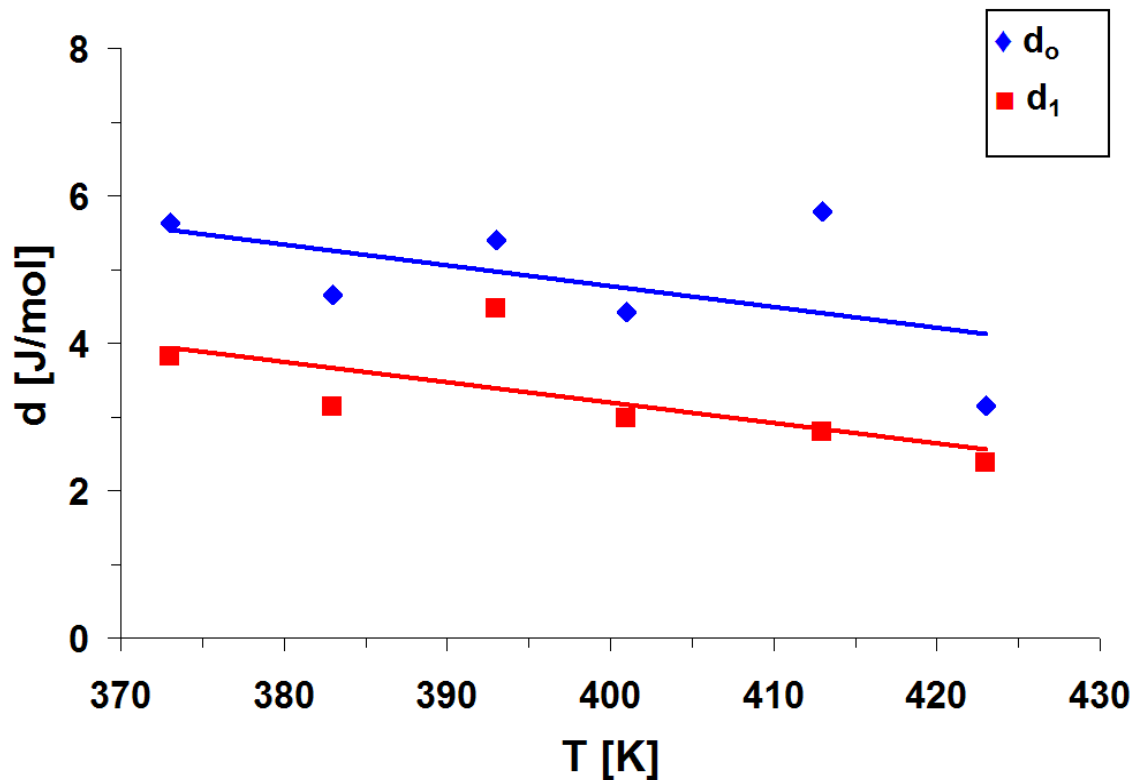


Fig. IV.4. Temperature dependence of the d_i quantities ($i=0,1$).

A similar relation holds for e_i . On the left hand side of (IV.2) all the quantities (and their temperature dependence) are known. It can be seen from Fig. IV.4. that

$d_o(T)$ and $d_l(T)$ are constant within the experimental errors, and their average value (about 4.0 ± 1.5 J/mol) is lower than the values of $d_o(\sigma)$ and $d_l(\sigma)$ shown on Fig. IV.2. On the other hand, $e_o(T)$ and $e_l(T)$ are temperature dependent with slopes -0.55 J/molK and -0.18 J/molK, respectively (Fig. IV.5.).

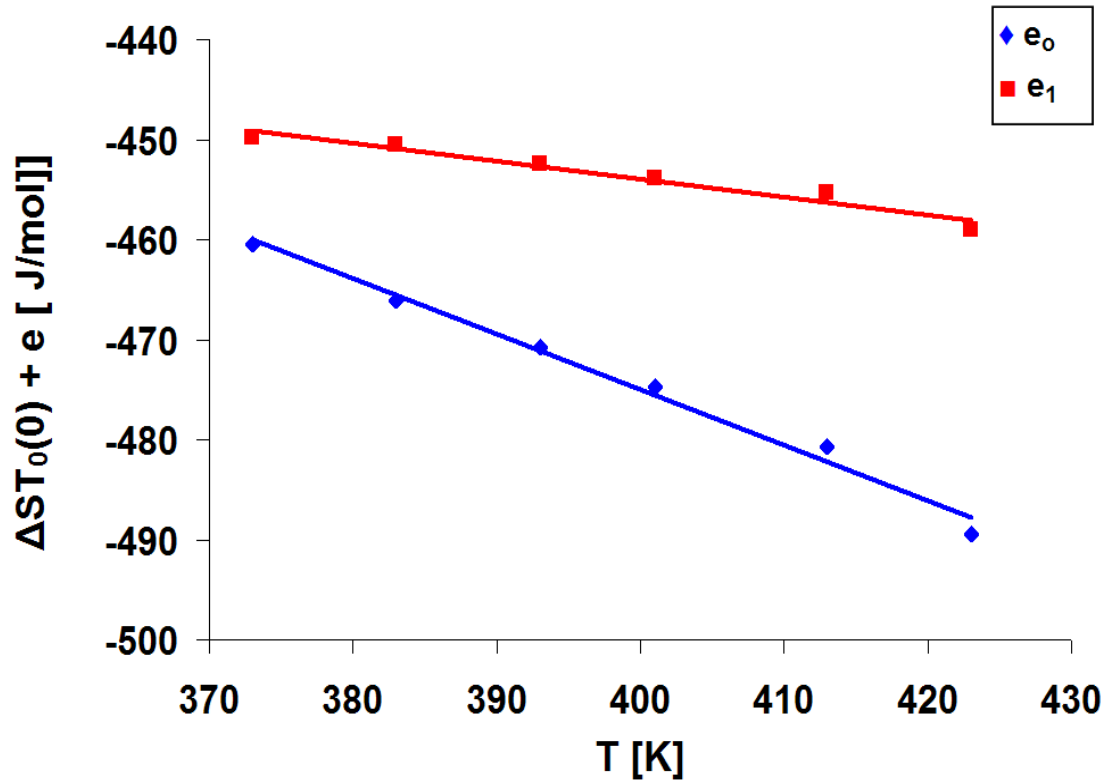


Fig. IV.5. Temperature dependence of the $T_0\Delta s + e_i$ quantities ($i=0,1$).

IV.1.4 Relations between the start and finish stresses and the test temperature

In order to get expression e.g. for $\sigma_{Ms}(T)$ let us take the first relations of (II.16) (at $\sigma=0$) and (II.17) and make the use of (II.12):

$$\begin{aligned} \sigma_{Ms}(T) = & - \left[\frac{\Delta s}{V \varepsilon^{lr}(\sigma_0(T))} \right] [T - M_s(0)] \\ & + \left[\frac{1}{V \varepsilon^{lr}(\sigma_{Ms})} \right] [d_0(\sigma_{Ms}) + e_0(\sigma_{Ms})] \\ & - \left[\frac{1}{V \varepsilon^{lr}(\sigma_0(T))} \right] [d_0(0) + e_0(0)]. \end{aligned}$$

(IV.3)

Note that in the relations used in obtaining (IV.3) the transformation strain and the martensite fraction derivatives of the dissipative and elastic terms were considered to be stress dependent. It can be seen that the relation (IV.3) will have the form usually found in the literature (see e.g. [IV.5, IV.6]) only if the sum of the last two terms is zero and, even in this case, it will have a linear temperature dependence only if $\varepsilon^{tr}(\sigma_o(T))$ is constant. Similar relations can be obtained for the other start and finish stresses. In the case of σ_{Mf} the difference of d_l and e_l appears in the second term, and ε^{tr} should be taken at σ_{Mf} , while for σ_{Af} and σ_{As} the e_o-d_o as well as e_l-d_l differences will be present. For example;

$$\begin{aligned} \sigma_{As}(T) = & - \left[\frac{\Delta s}{V \varepsilon^{tr}(\sigma_o(T))} \right] [T - A_s(0)] \\ & + \left[\frac{1}{V \varepsilon^{tr}(\sigma_{As})} \right] [e_1(\sigma_{Ms}) - d_1(\sigma_{Ms})] \\ & - \left[\frac{1}{V \varepsilon^{tr}(\sigma_o(T))} \right] [e_1(0) - d_1(0)]. \end{aligned} \quad (IV.4)$$

One can recognize from (IV.3) or (IV.4) that interestingly if the contributions from the elastic and dissipative contributions are neglected, the slopes of all start and finish stresses versus temperature have the same value.

It can be seen that the functions on Fig. III.10. can be approximated by straight lines and Table III.1 contains their slopes. However, while the slopes of $\sigma_{Ms}(T)$ and $\sigma_{Af}(T)$ as well as $\sigma_{Mf}(T)$ and $\sigma_{As}(T)$ are the same, the slopes of these two groups differ from each other more than the estimated error (about 0.05 MPa/K [IV.4]).

In (IV.3) and (IV.4) both d_o and d_l terms are practically temperature independent [III.4] while $e_o(\sigma_{Ms}(T))$ depends on temperature (Fig. IV.5: $\partial e_o/\partial T = -0.50$ J/molK, $\partial e_l/\partial T = -0.18$ J/molK [IV.4]). Furthermore, the $\varepsilon^{tr}(\sigma_o(T))$ and $\varepsilon^{tr}(\sigma_{Ms}(T))$ functions should be considered in the temperature interval 373-425K (Figs. III.7 and III.10) i.e. $\varepsilon^{tr}(\sigma_o(T)) \cong \varepsilon^{tr}(\sigma_{Ms}(T)) \cong 0.055$. Thus, the terms containing $1/V\varepsilon^{tr}$ will be approximately constant $1/V\varepsilon^{tr} \cong 2.3 \times 10^6$ mol/m³ (a bit larger than the value belonging to $V\varepsilon^{tr}_{max}$: 2.1×10^6 mol/m³).

Thus, one can estimate the contributions of the 1st, 2nd and 3rd terms in (IV.3) and (IV.4) to the slope of σ_{Ms} vs. T function (Table IV.1). The slope of the third term is 0 ($\varepsilon^{tr}(\sigma_o(T)) \cong \varepsilon^{tr}(\sigma_{Ms}(T)) \cong const.$) and from *the second term only the elastic term*

contributes to the slope. This also explains why the slopes of σ_{Ms} and σ_{Af} as well as σ_{Mf} and σ_{As} are similar, because they contain the temperature derivatives of e_o and e_l , respectively.

It is worth mentioning that it was already mentioned in [IV.4] that the d_i ($i=0,1$) values have a decreasing tendency with increasing temperature, but the slope was not estimated because of the relatively high experimental errors. Now if we put straight lines to the points in Fig. IV.4. we get for both slopes -0.028 J/molK, which leads to a -0.064 MPa/K contribution from the 3rd term in (IV.3) or (IV.4), which is just around the experimental error of the slopes in Fig. III.10. Taking all the contributions into account *the agreement between the estimated and experimental values is very good.*

Experimental [IV.4]		σ_{Ms} vs. T	σ_{Mf} vs. T	σ_{Af} vs. T	σ_{As} vs. T
Slope in MPa/K		1.6	2.0	1.5	2.2

Estimated (parts)	Eq. (II.12)	1 st term in (IV.3) & (IV.4)	2 nd term in (IV.3) e_o	2 nd term in (IV.4) e_l	3 rd term in (IV.3) or (IV.4) $d_0=d_l$
Slope in MPa/K	2.59	2.83	-1.15	-0.41	0 or -0.028

Estimated (whole)	σ_{Ms} vs. T	σ_{Mf} vs. T	σ_{Af} vs. T	σ_{As} vs. T
Slope in MPa/K	1.68 or 1,65	2.42 or 2.45	1.68 or 1.65	2.42 or 2.45

Table IV.1. Experimental and estimated values of the slopes of the start and finish stresses versus T.

IV.1.5 Self-consistency of our analysis

The following facts confirm the self-consistency of the analysis carried out above. In both sets of investigations (thermally and stress induced transformations) we have observed that the transformation strain depends on the field parameter (Figs. III.5. and III.7.), but both have the same saturation value. This can be interpreted by the increase of the fraction of the stress-induced (single) martensite variant structure, η , according to relation (IV.1), from which e.g. an S-shape $\eta(\sigma)$ function follows.

The difference of the slopes of the linear stress dependence of the start and finish temperatures as well as the slope of the T_o temperature corresponds to the contribution from the stress dependence of the elastic energy terms (the dissipative terms are practically independent of σ).

The values obtained for the d_o and d_l quantities have almost the same values in both sets, but their value is lower for the ε - σ loops by a factor of 3. It is worth mentioning that most probably both $d_i(\sigma)$ and $d_i(T)$ ($i=0,1$) functions are not constant but the resolution of their dependence on σ and T , respectively, due to their small values and the experimental errors, is not possible from our data. Nevertheless, Fig. IV.2. (and Fig. IV.7. showing D versus σ) suggest that the $d_i(\sigma)$ function could have a maximum at about 60 MPa, while at $\sigma=0$ MPa as well as at $\sigma=178$ MPa its average value is about 6-7J/mol, which is close to 4 J/mol obtained from the $d_i(T)$ functions. Furthermore, since at higher temperatures higher stress is necessary to start the transformation, it is also plausible that the negative slope of the second part on Fig. IV.2. should correspond to a negative slope on the $d_i(T)$ functions. Indeed, there is a slight decreasing tendency with increasing T on Fig. IV.4. Unfortunately, the accuracy of our present results does not allow a deeper and proper analysis of the field dependence of the dissipative terms. In addition, the details of the transformation (and thus the magnitude of d_i) can be different for stress and temperature induced transformations as well as can also depend on the prehistory of the samples (not investigated here).

IV.1.6 Stress and temperature dependence of the total dissipative, D , and elastic energy, E

IV.1.6.1 Stress dependence

Fig. IV.6. shows the $d(\xi)$ function calculated from the inverses of the normalized hysteresis ε - T loops (see relations (II.6) and appendix 1) at different stresses. In Fig. IV.7. the twice of the integral of $d(\xi)$ function for the whole thermal cycle (i.e. between $\xi=0$ and $\xi=1$), $D(\sigma)$ is plotted versus σ . The full dots in Fig. IV.7. show the values obtained from integration, while the open dot at $\sigma=0$ was calculated from the DSC curves (Fig. III.3.) according to the relation $Q^\downarrow + Q^\uparrow = 2D$ ($Q^\downarrow = -331.6$ J/mol, $Q^\uparrow = 357.6$ J/mol). It can be seen that full dots fit self-consistently within the experimental errors to the open dot calculated from the independent (DSC) measurement. Again we can see the maximum of the dissipative energy around 60 MPa. Nevertheless, the value of D can be taken to be constant within the experimental scatter and its average is about 12 J/mol [IV.7].

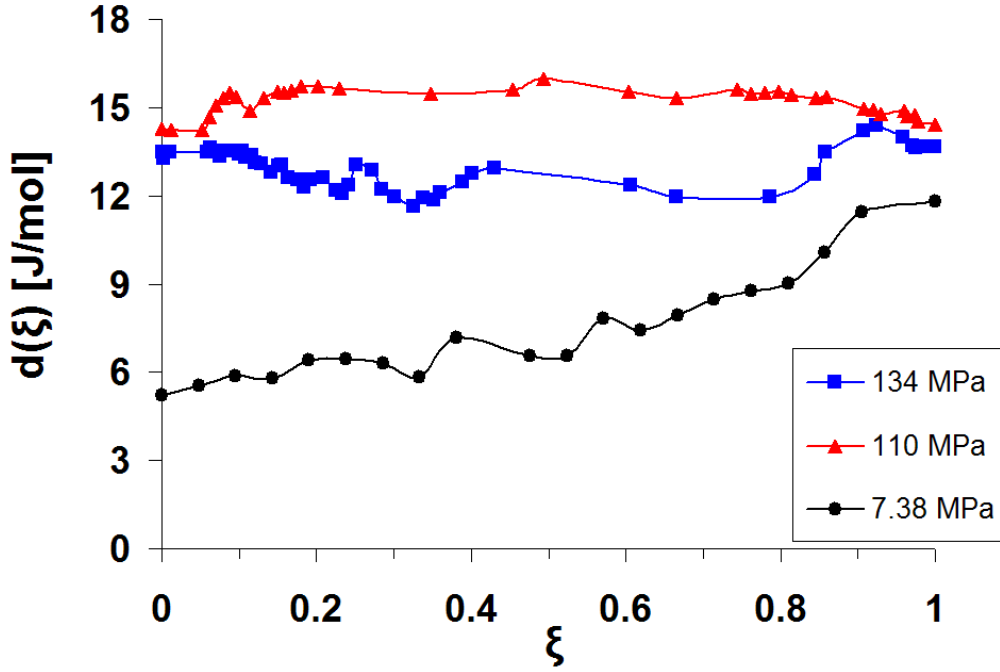


Fig. IV.6. Dissipative energy ($d(\xi) = [d_0\xi + d_1(\xi)]/2$) term versus the transformed martensite fraction, calculated from the normalized ε - T loops, at different stress levels.

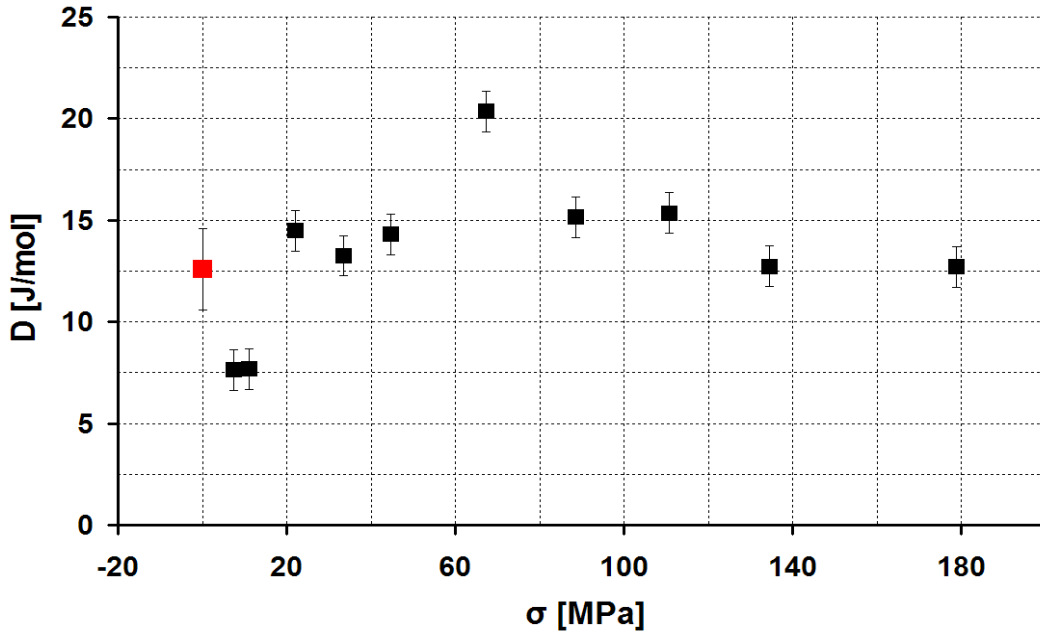


Fig. IV.7. Energy dissipated within one ε - T hysteresis loop as the function of σ .

Fig. IV.8. shows the $T^{\downarrow}(\xi) + T^{\uparrow}(\xi) = 2T_0(\sigma) + 2e(\xi, \sigma)/[-\Delta s]$ vs. ξ functions calculated from the ξ - T curves at different stresses. It can be seen that the curve at zero stress, calculated from the DSC measurement, fits self-consistently to the others.

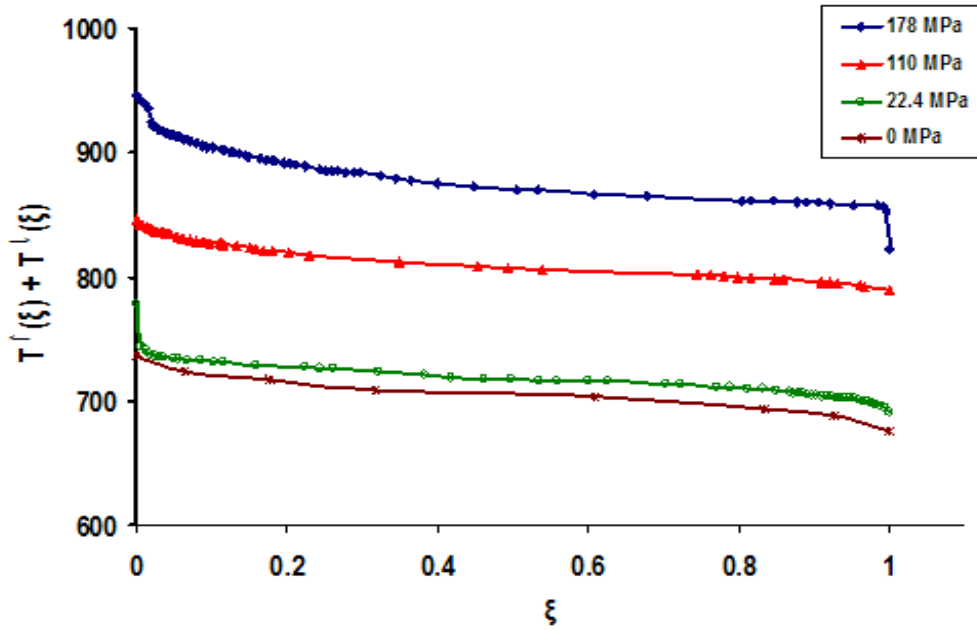


Fig. IV.8. $T^{\downarrow}(\xi) + T^{\uparrow}(\xi)$ vs. ξ at different stresses.

Fig. IV.9. shows the integrals of the curves of Fig. IV.8. giving the total elastic energy, E , per one cycle (irrespective of the constant $\Delta s T_0$ value). We can see that the total elastic energy decreases with increasing applied uniaxial stress. This is because the stored elastic energy can be at lowest value when the martensite phase has only one variant due to the high stress.

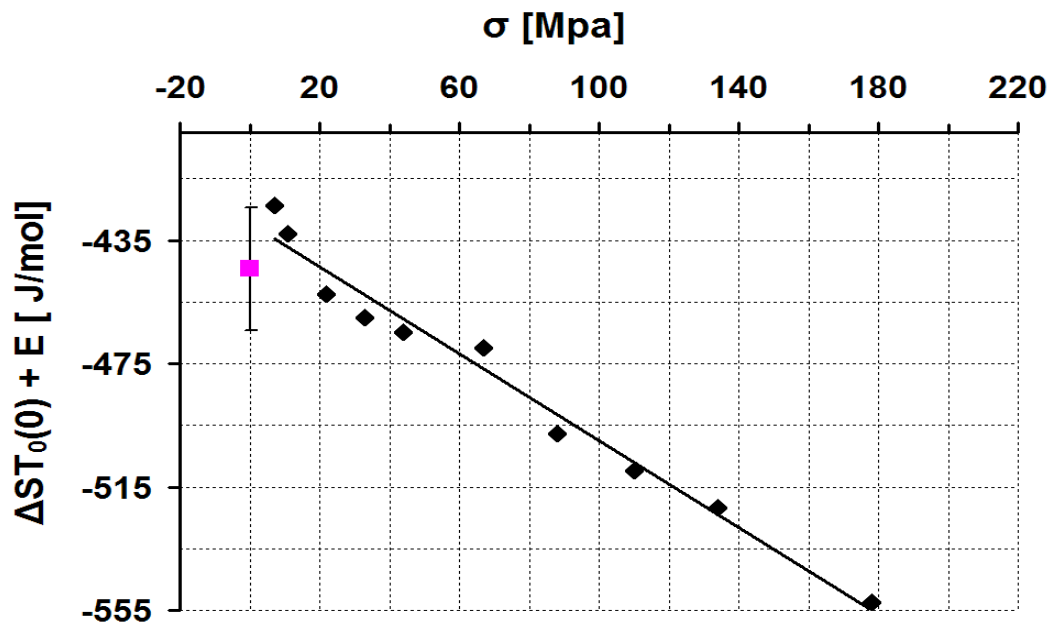


Fig. IV.9. Stress dependence of the total elastic energy, E . The point at zero stress is obtained from the DSC data.

IV.1.6.2 Thermal Dependence

The functions

$$\sigma^{\downarrow}(\xi) - \sigma^{\uparrow}(\xi) = 2d(\xi, T)/V \varepsilon^r(\sigma) \text{ and } \sigma^{\downarrow}(\xi) + \sigma^{\uparrow}(\xi) = 2\sigma_o(T) + 2e(\xi, T)/V \varepsilon^r(\sigma) \text{ vs. } \xi$$

functions were plotted at different temperatures. The integrals of these functions give the total dissipative energy, $2D(T)$, and the $2E(T) + 2T_o(0)\Delta s$ quantity, containing total elastic energy [IV.8]. These functions are plotted in Figs. IV.10. and IV.11. From Fig. IV.10. we can see that the dissipative energy has no temperature dependence, and its value scatters within the experimental errors around 7 J/mol. On other hand the elastic energy has strong temperature dependence (Fig IV.11.). Since the $T_o(0)\Delta s$ quantity is negative ($\Delta s < 0$), from the fact that the values on the vertical axis are negative it can be concluded that $E(0) < |T_o(0)\Delta s|$. Furthermore, it is clear from the sign of the slopes in Fig. IV.11. that E decreases with increasing temperature.

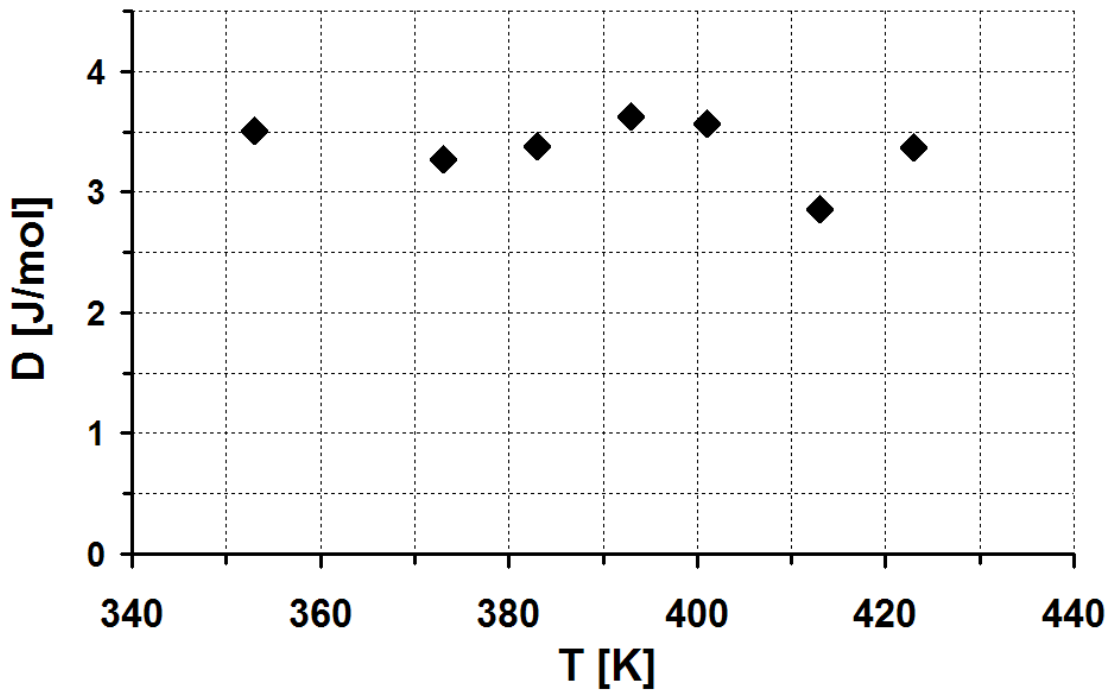


Fig. IV.10. Temperature dependence of the total dissipative energy, D .

This is quite plausible because the elastic energy can be larger for thermally induced (random) multi-variant structure, because in this case the overlapping of elastic fields of the differently oriented variants leads to more remarkable elastic energy accumulation.

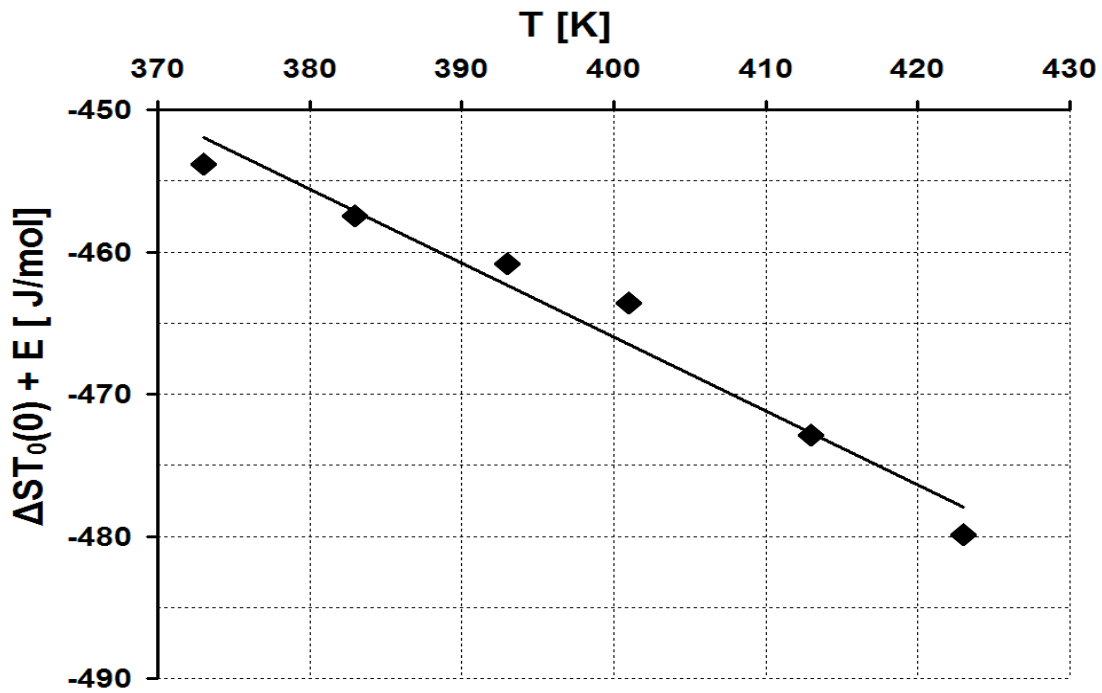


Fig. IV.11. Temperature dependence of the total elastic energy, E .

IV.1.7 Dependence of the dissipative and elastic energies on the number of cycles

The results presented in this chapter were published in [IV.9].

IV.1.7.1 Thermal cycling

The slopes of the up and down branches as well as the area of the hysteresis curves in Fig.III.12. show changes with increasing number of cycles: the lower area indicates lower dissipative energy contribution and larger slopes show larger elastic energy contribution (Fig.IV.12. and Fig.IV.13.). The ξ dependence of the elastic and dissipative energy can be obtained from the sum and difference of T^\uparrow and T^\downarrow curves in Fig. III.12. (see eq. (II.6)), respectively. Fig.IV.12. and Fig.IV.13. show how the total elastic (E), and the total dissipative (D) energy, change with the number of cycles, as calculated from the integrals of the above curves (between $\xi=0$ and $\xi=1$), versus N . We can get E and D by using the well-known relations $Q^\downarrow + Q^\uparrow = 2D$ and $Q^\downarrow - Q^\uparrow = 2E + 2T_0\Delta S$ as well. These results fit well to the points calculated from the above integrals (see Figs.IV.12. and Fig.IV.13.).

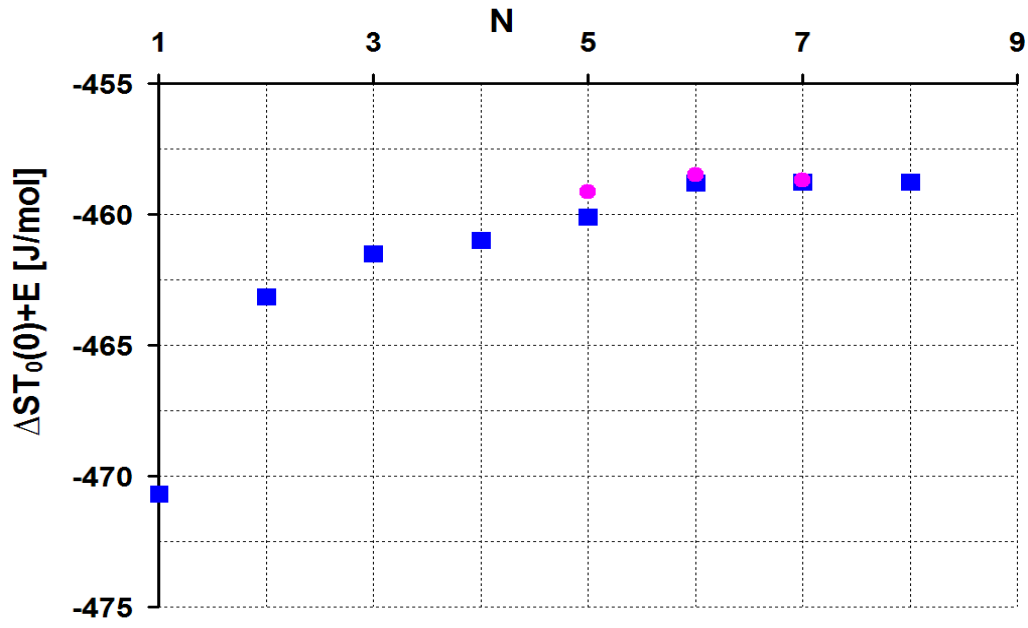


Fig. IV.12. Total elastic energy as the function of number of cycles for thermal loops (■ from the ξ -T loops, ● from the heats of transformation).

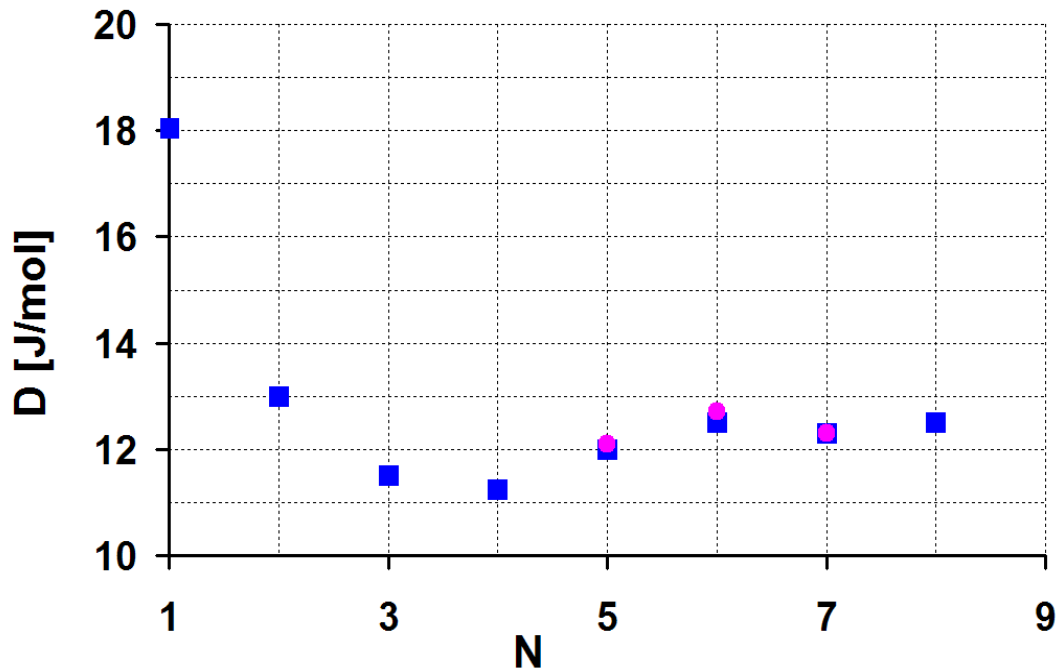


Fig. IV.13. Total dissipative energy as the function of number of cycles for thermal loops (■ from the ξ -T loops, ● from the heats of transformation).

IV.1.7.2 Mechanical cycling

The elastic and the dissipative energies were calculated from Fig III.13. using the relations of the integrals of $\sigma^\downarrow(\xi)+\sigma^\uparrow(\xi)$ and $\sigma^\downarrow(\xi)-\sigma^\uparrow(\xi)$ respectively. Fig IV.14. and Fig IV.15. show the N dependence of calculated total elastic energy as well as total dissipative energy, respectively.

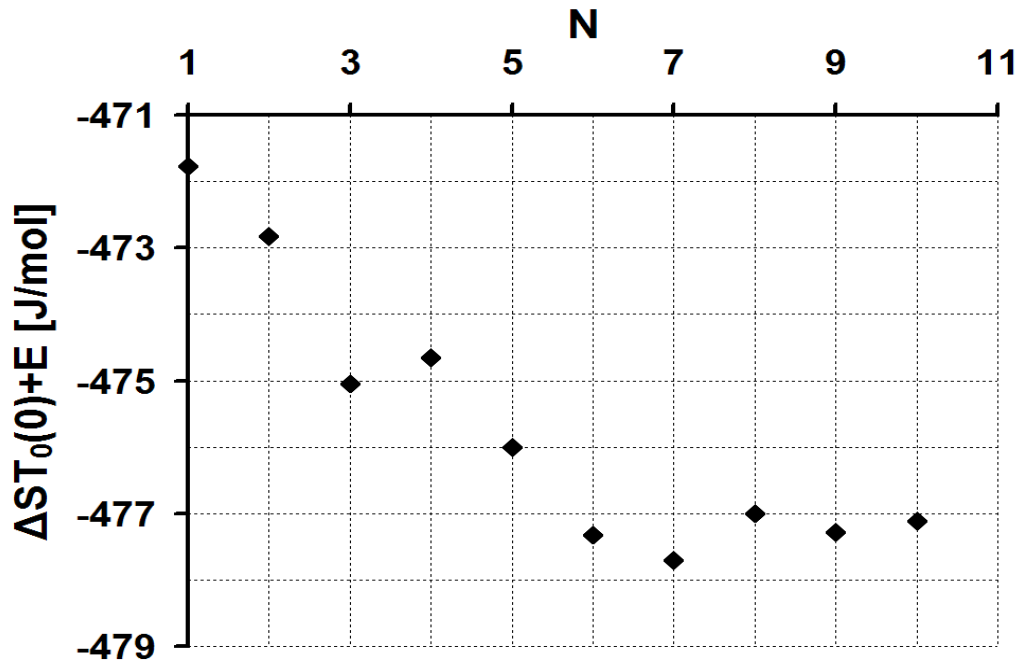


Fig. IV.14. Total elastic energy versus the number of cycles.

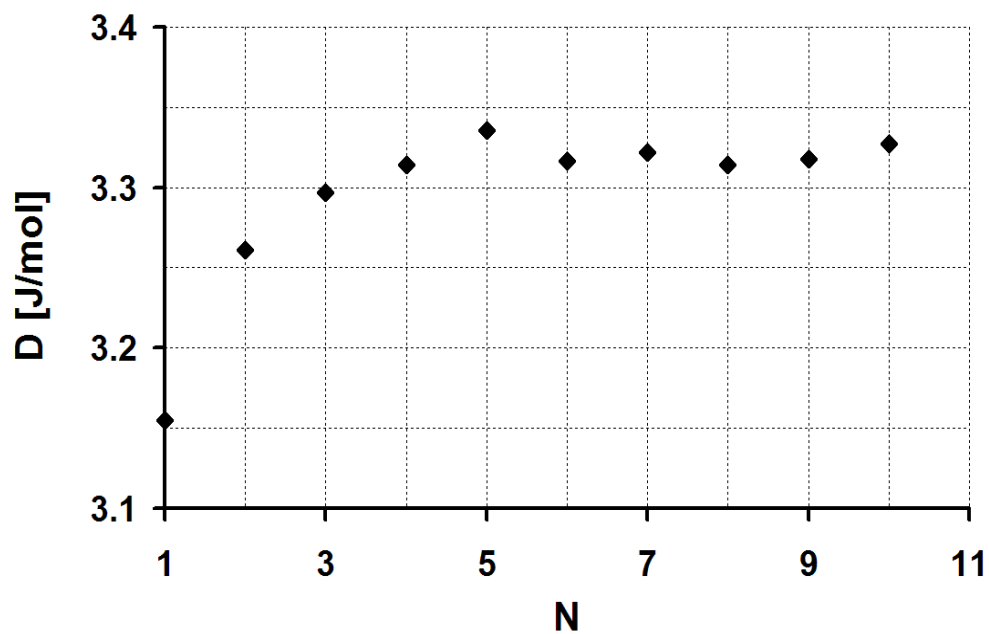


Fig. IV.15. Total dissipative energy as the function of number of cycles.

In the calculations of E and D the σ dependence of ε'' on N was neglected and $\varepsilon''=0.046$ was taken (as read out from the curves in Fig. III.5. which is also in a good accordance with the value obtained from the temperature dependence of ε'' at 373K (see Fig III.7.). It is clear that the elastic energy decreases before reaching a constant value after few cycles, while the dissipative energy increases by increasing N and saturates after a few mechanical cycles.

IV.7.3 Results on polycrystalline samples

The elastic and dissipative energy contributions as the function of stress are plotted in Figs. IV.16. and IV.17., respectively for the CuAl(11,6wt%)Be(0.36wt%) samples. (Here we investigated only the $T(\varepsilon)$ loop and the effect of thermal cycling). One can see that the elastic energy decreases with increasing applied uniaxial stress and it reaches a saturation value at high enough stresses. On other hand, the dissipative energy increases and saturates at high stresses.

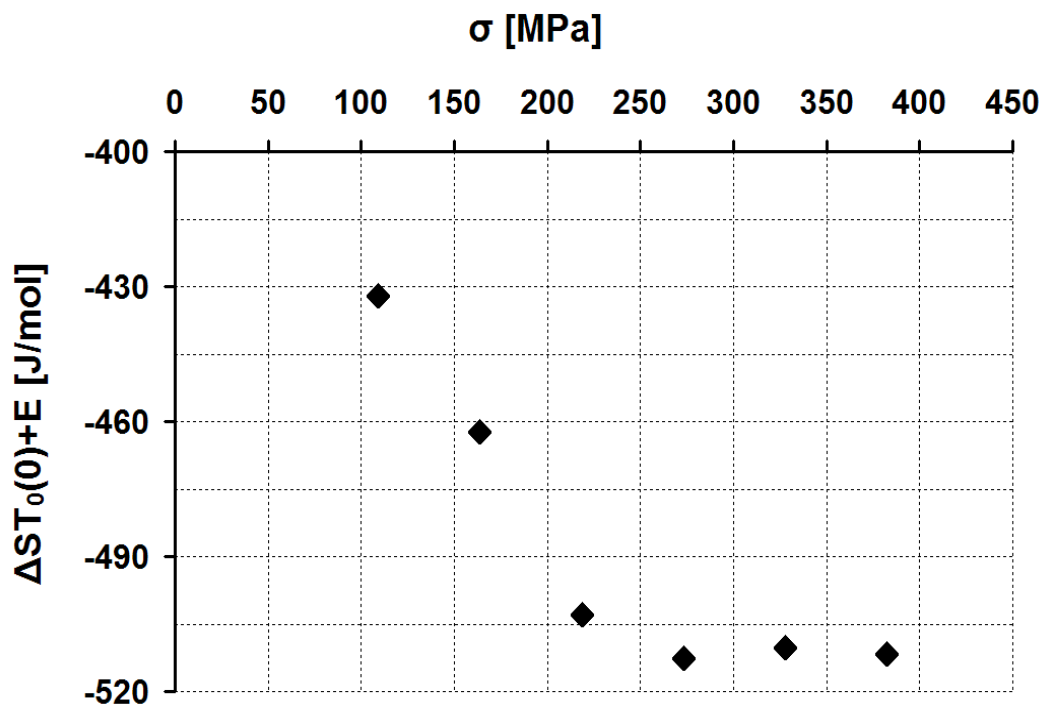


Fig. IV.16. Total elastic energy as a function of the applied stress.

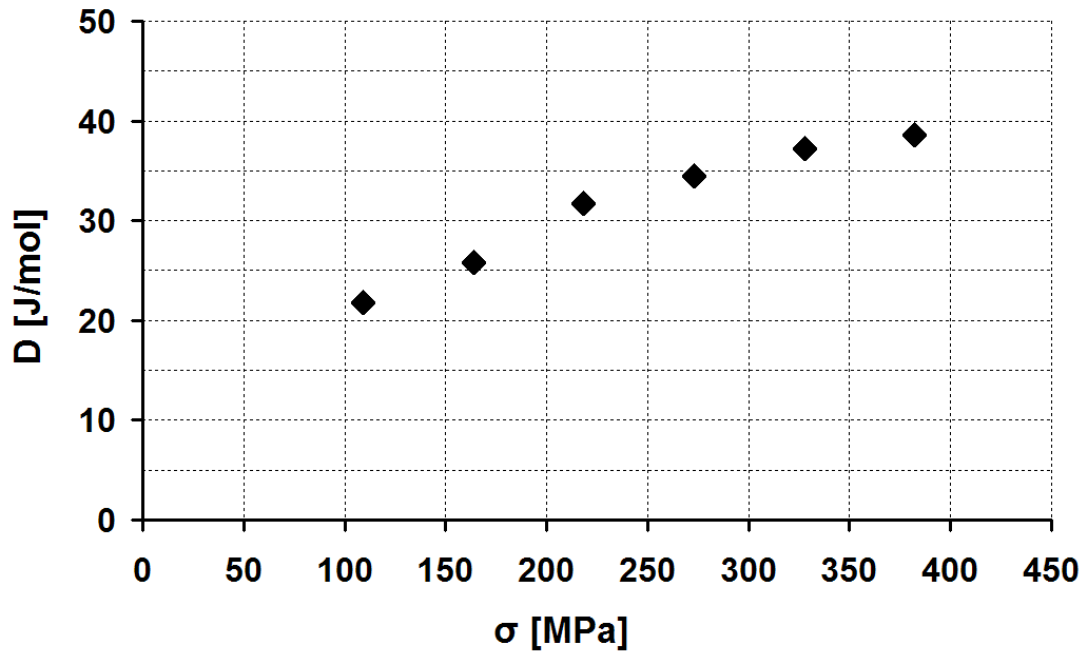


Fig. IV.17. Total dissipative energy as a function of the applied stress.

The effect of thermal cycling on the DSC curves is shown in Fig. IV.18. and it can be seen that there is no cycling-effect at zero stress.

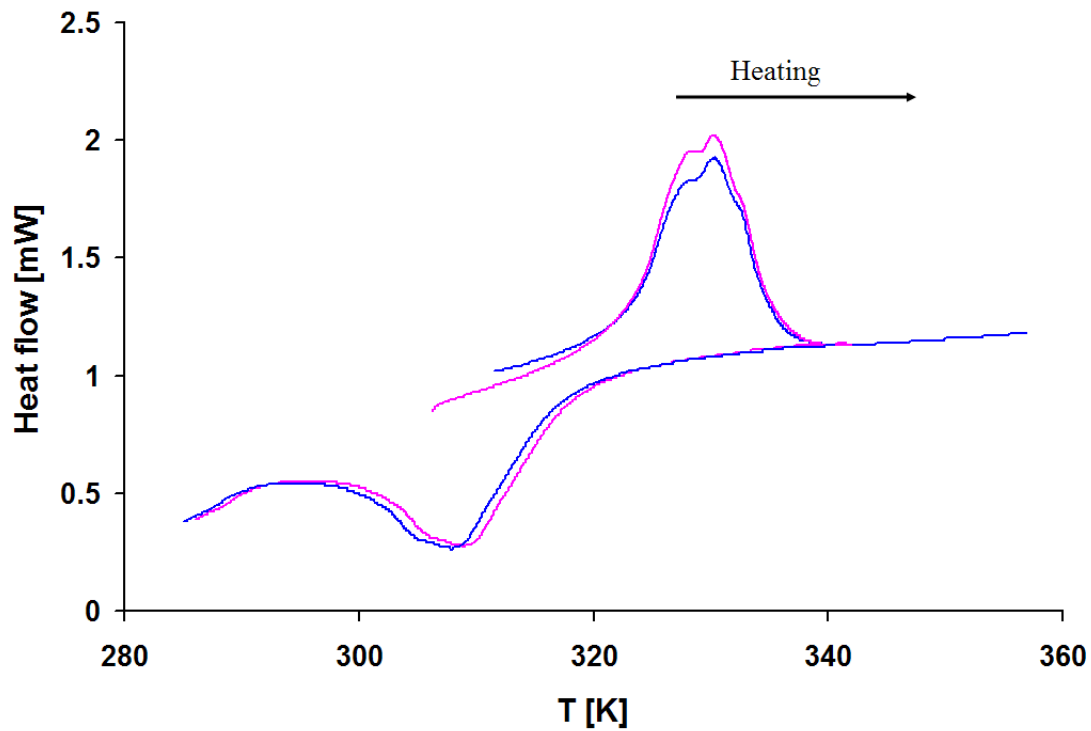


Fig. IV.18. Thermal cycling effect on the CuAl(11,6wt%)Be(0.36wt%) polycrystalline shape memory alloy.

References

- [IV.1] D.L. Beke, L. Daróczy, Z. Palánki, *Proc. of Int. Conf. on Shape memory and Superelastic Technologies*, 2007 Tsukuba, Japan, edited by S. Miyazaki (ASM International, Materials Park, Ohio, (2008) 607.
- [IV.2] Z. Palánki, L. Daróczy, and D.L. Beke, *Mater. Trans.*, A46 (2005) 978.
- [IV.3] A. Planes, T. Castan, J. Ortin, L. Delay, *J. Appl. Phys.* 66 (6) (1989) 2342.
- [IV.4] T.Y. El Rasasi, L. Daróczy, D.L. Beke, *Intermetallics* 18 (2010) 1137.
- [IV.5] L. Delaey, *Diffusionless transformations*” in R.W. Cahn, P.Haasen and E.J. Kramer (editors) „*Materials Science and Technology – A Comprehensive Treatment*” Vol. 5. P. Haasen (ed.) *Phase Transformations in Materials*, (Weinheim, VCH, 1991) 339.
- [IV.6] H. Kato and S. Miura, *Acta metall. Mater.* 43 (1) (1995) 351.
- [IV.7] T.Y. El Rasasi, L. Daróczy, D.L. Beke, *Materials Science Forum.* 659 (2010) 399.
- [IV.8] T.Y. El Rasasi, L. Daróczy, D.L. Beke, submitted to *Materials Science Forum.*
- [IV.9] T.Y. El Rasasi, L. Daróczy, D.L. Beke, in print in *J. Alloy and Compunds.*

Chapter V

Summary

Two types of high temperature Cu-based shape memory alloys have been investigated: CuAl(11.5wt%)Ni(5.0wt%) single crystalline and CuAl(11,6wt%)Be(0.36wt%) polycrystalline samples. Our main goal was the determination of the non-chemical energy contributions (e.g. the elastic and dissipative energy contributions) to the martensitic phase transformations during thermal and stress induced cycling. In both alloys only the transformation from the high temperature cubic β phase to the β' (18R) phase takes place at the investigated compositions.

I. CuAl(11.5wt%)Ni(5.0wt%) single crystal

Two separated sets of measurements have been carried out investigating the characteristic parameters; i) determination of the martensite fraction-temperature $\xi(T)$ curves at different constant stresses; ii) strain-stress $\varepsilon(\sigma)$ hysteresis curves at different constant temperatures ($\varepsilon \sim \xi$).

From the measurements of (ε -T) and the (ε - σ) hysteresis curves, the stress and the temperature dependences of the transformation strain (ε^{tr}) was determined [V.1]. The transformation strain, ε^{tr} , determined from the σ - ε loops at constant temperatures, shows a saturation value of about 6.1%, close to the theoretic maximal value. As it is expected, the same saturation value was obtained from the $\varepsilon(T)$ loops. The stress and temperature dependence of ε^{tr} is interpreted by the gradual change of the martensite structure formed: at higher uniaxial stress values more oriented martensite variants develop with higher resultant strain.

From the DSC curves we could calculate the entropy of the examined alloy as well as we could obtain the $\varepsilon(T)$ hysteresis curve at zero stress.

By using the model developed from our laboratory, the derivatives of the non-chemical free energy contributions, by the martensite volume fraction (ξ), to the phase transformation at fixed temperatures as well as at fixed stresses have been calculated. These contributions were calculated from the $\xi(\sigma)$ hysteresis curves at constant temperatures and $\xi(T)$ loops at constant stresses.

It was obtained that: [V.1 – V.4]

- The derivatives of the elastic energy by the martensite volume fraction, ξ , have strong temperature and stress dependence;
- The derivatives of the dissipative energy were practically constant, or the changes were almost within the experimental errors;
- The elastic energy, calculated from the start and finish temperatures of the ξ -T hysteresis curve at zero stress obtained from the DSC curve, fits very well to the straight lines obtained for the start and finish temperatures of the ξ -T hysteric curves at different $\sigma \neq 0$ levels;
- The slopes of the start and finish stresses versus temperature as well as the start and finish temperatures versus stress functions are different from the slopes of the equilibrium transformation stress versus temperature, $\sigma_0(T)$, as well as of the equilibrium transformation temperature versus stress, $T_0(\sigma)$, functions, respectively. It is shown that this is due to the temperature as well as stress dependence of the elastic energy contributions;
- The total dissipative and total elastic energy contributions were also calculated from the integrals of their derivatives. Both the stress and temperature dependence of the total elastic energy per cycle show a linear dependence in the range investigated with slopes -1.30 J/mol MPa and -1.04 J/mol K, respectively. The total elastic energy (E) decreases with increasing stress in accordance with the increasing volume fraction of the well oriented single variant structure;
- The total dissipative energy (D) does not show any stress or temperature dependence. The value of $D(\sigma)$ is constant within the experimental scatter and its average is about 12 J/mol, and the average value of $D(T)$ is about 7 J/mol.

Mechanical and thermal cycling on the CuAl(11.5wt%)Ni(5.0wt%) single crystal shape memory alloy have been carried out to see the effect of the cycling on the contributions of the elastic and the dissipative energy in the phase transformations. The following results were obtained [V.5]:

- Both the dissipative (D) and elastic energy (E) show a definite dependence on the number of cycles in the first few cycles and then a saturation value is reached with increasing N. i.e. the stress-strain and strain-temperature responses stabilize;
- In thermal cycling the elastic energy, E, as well as the dissipative energy, D per one cycle increases as well as decreases, respectively with increasing number of cycles, while in mechanical cycling there is an opposite tendency. These changes are related to the change in the martensite variant structure during cycling.

II. CuAl(11,6wt%)Be(0.36wt%) polycrystalline shape memory alloy

Similar set of measurements, as carried out for CuAl(11.5wt%)Ni(5.0wt%) single crystalline samples, were carried out in CuAl(11,6wt%)Be(0.36wt%) polycrystalline samples. But only the ϵ -T loops were measured at different stress levels and the effect of cycling was investigated.

- It was obtained that the elastic energy decreases with increasing applied uniaxial stress and it reaches a saturation value at high enough stresses. On other hand the dissipative energy increases and saturates at high stresses.
- No thermal cycling effect has been detected on the DSC curves measured at zero σ .

References

- [V.1] T.Y. El Rasasi, L. Daróczy, D.L. Beke, *Intermetallics*. 18 (2010) 1137.
- [V.2] D.L. Beke, T.Y. El Rasasi, L. Daróczy, *ESOMAT 2009*, 02002 (2009)
DOI:10.1051/esomat/200902002 ©
- [V.3] T.Y. El Rasasi, L. Daróczy, D.L. Beke, *Materials Science Forum*. 659 (2010) 399.
- [V.4] T.Y. El Rasasi, L. Daróczy, D.L. Beke, submitted to the *Materials Science Forum*.
- [V.5] T.Y. El Rasasi, L. Daróczy, D.L. Beke, in print in *J. Alloys and Compounds*

Magyar nyelvű összefoglaló

A dolgozat fő célkitűzése a martenzites átalakulásokat leíró szabadenergia függvények nem kémiai (rugalmas és disszipatív) részének a vizsgálata volt termikus, és feszültség indukált átalakulások során. Munkám során magas átalakulási hőmérsékletű réz alapú ötvözeteken végeztem kísérleteket. Vizsgáltam a nem kémiai szabadenergia tagok viselkedését egykristály (CuAl(11.5wt%)Ni(5.0wt%)) valamint polikristályos (CuAl(11.6wt%)Be(0.36wt%)) mintákon. Mindkét ötvözetben csak a $\beta \rightarrow \beta'$ (18R) szerkezeti fázisátalakulás játszódik le a vizsgált összetételeknél.

I. CuAl(11.5wt%)Ni(5.0wt%) egykristály minták

Két különálló mérési sorozatban vizsgáltam a következő jellemzőket: i) konstans egytengelyű feszültség értékek mellett meghatároztam az átalakult martenzit hányad-hőmérséklet (ξ -T) görbéket; ii) állandó hőmérsékleten mértem a relatív megnyúlás feszültség (ε - σ) görbéket ($\varepsilon \sim \xi$).

A (ξ -T) valamint (ε - σ) hiszterézis görbékből meghatároztam az átalakulási deformáció (ε^{tr}) feszültség és hőmérséklet függését [V.1]. Az ε - σ hurkokból meghatározott ε^{tr} értéke 6.1%-nál, amely közel van az elméletileg várható maximális értékhez, telítést mutat. Mint ahogy várható volt, ugyanez a telítési érték adódott az ε -T görbékből is. ε^{tr} feszültség és hőmérséklet függését a martenzit variáns szerkezetének fokozatos változásával magyaráztam: nagyobb egytengelyű feszültségeknél egy jobban (egyirányban) rendezett variáns szerkezet alakul ki, melyhez nagyobb visszamaradó deformáció tartozik.

A DSC görbékből ki tudtam számítani az átalakuláshoz tartozó entropiát, valamint nulla feszültséghez tartozó (ε -T) görbét is meg tudtam határozni.

A fázis átalakulásokhoz tartozó nem-kémiai szabadenergia járulékok átalakult anyaghányad szerinti deriváltjainak hőmérséklet és feszültségfüggését a (ξ -T) és (ξ - σ) függvényekből számítottam ki, a tanszéken korábban publikált modell felhasználásával.

A főbb eredmények a következők [V.1 – V.4]:

- A rugalmas szabadenergia járulékok átalakult anyaghányad szerinti deriváltjai erős hőmérséklet és feszültségfüggést mutatnak.

- A disszipatív szabadenergia deriváltak nem mutattak mérhető hőmérséklet ill. feszültségfüggést.
- A DSC görbékből nyert (ξ -T) függvények kezdeti- és vég-hőmérsékleteiből kiszámítottam az elasztikus energia-deriváltak értékeit. Ugyanezen értékek feszültségfüggését is meghatároztam a megnyúlásmérésekből 0-tól különböző húzófeszültségeknél. A megnyúlásmérésekből $\sigma=0$ feszültségre extrapolált, valamint a DSC mérésből kapott értékek jó egyezést mutatnak, ami a kiértékelési módszer önkonzisztens voltát bizonyítja.
- A transzformációk kezdeti- és vég- hőmérsékleteit a feszültség függvényében ábrázolva azt tapasztaltam, hogy ezen görbék meredeksége eltér a termodinamikai egyensúlyi hőmérséklet feszültségfüggését megadó görbe meredekségétől. Hasonló jelenség tapasztalható a kezdeti- és vég-feszültségek valamint az egyensúlyi feszültség hőmérsékletfüggését vizsgálva is. Megmutattam, hogy ez a rugalmas energia járulékok hőmérséklet és feszültség függésével áll összefüggésben.
- A rugalmas és disszipatív szabadenergia deriváltak integrálásával kiszámítottam a teljes transzformációhoz tartozó rugalmas és disszipatív energiákat. A E teljes rugalmas energia a feszültség illetve a hőmérséklet függvényében lineáris függést mutat -1.30J/molMPa , illetve -1.04 J/molK meredekségekkel. Az rugalmas energia csökkenése a feszültség növelésekor azzal magyarázható, hogy egyre jobban orientált egyre kevesebb variánsból álló martenzit szerkezet jön létre.
- Nem tapasztalható feszültség vagy hőmérsékletfüggés a teljes ciklusra számított disszipatív energia (D) esetében. A feszültség függvényében mérve (a hőmérsékleti hurkokból számolt) $D(\sigma)$ átlagértéke 12J/mol -nak míg a hőmérséklet függvényében (a feszültségi hurkokból számolt érték) 7J/mol -nak adódott.

Az egykristály mintákat mechanikai és termikus ciklizálásnak alávetve az alábbi eredményeket kaptam [V.5]:

- Mind a rugalmas, mind a disszipatív energia erősen változik az első néhány ciklus során majd nagyobb ciklusszámoknál tart egy telítési értékhez.

- Termikus ciklizálás során a rugalmas energia növekvő ciklusszámmal nő a disszipatív energia pedig csökken. Mechanikus ciklizálás során a fentivel ellentétes tendenciát figyeltem meg. Ezek a változások a martenzit variáns-szerkezet ciklizálás során bekövetkező átrendeződésének tulajdoníthatók.

II. CuAl(11,6wt%)Be(0.36wt%) polikristályos minták

Az egykristály mintákon elvégzettekhez hasonló termikus ciklizálást végeztem polikristályos szerkezetű (CuAl(11.6wt%)Be(0.36wt%)) összetételű anyagokon különböző húzófeszültségek mellett, de itt csak az $\varepsilon \sim T$ görbékét mértem különböző feszültségeknél valamint a ciklizálásnak ezekre gyakorolt hatását vizsgáltam.

Eredmények:

- Az elasztikus energia növekvő feszültségek hatására csökken, nagy feszültség szinteknél egy telítési értékhez tart. A disszipatív energia hasonló, de ellentétes tendenciájú változást mutat.
- A termikus ciklizálás a DSC görbéken nem okozott megfigyelhető változást.

References

- [V.1] T.Y. El Rasasi, L. Daróczy, D.L. Beke, *Intermetallics*. 18 (2010) 1137.
- [V.2] D.L. Beke, T.Y. El Rasasi, L. Daróczy, *ESOMAT 2009*, 02002 (2009)
DOI:10.1051/esomat/200902002 ©
- [V.3] T.Y. El Rasasi, L. Daróczy, D.L. Beke, *Materials Science Forum*. 659 (2010) 399.
- [V.4] T.Y. El Rasasi, L. Daróczy, D.L. Beke, submitted to the *Materials Science Forum*.
- [V.5] T.Y. El Rasasi, L. Daróczy, D.L. Beke, in print in *J. Alloys and Compounds*

List of Publications:

- 1- D.L. Beke, **T.Y. El Rasasi**, L. Daróczy, "On the temperature and stress dependence of transformation strain in single crystalline Cu-Al-Ni shape memory alloys" **ESOMAT 2009**, 02002 (2009) DOI:10.1051/esomat/200902002 ©
- 2- **T.Y. El Rasasi**, L. Daróczy, D.L. Beke, "On the relation between the martensite start stress and the temperature in single crystalline Cu-11.5wt%Al-5.0wt%Ni shape memory alloy", **Materials Science Forum**, 659 (2010) 399. (IF.: 0.000)
- 3- **T.Y. El Rasasi**, L. Daróczy, D.L. Beke, "Investigation of thermal and stress induced hysteresis curves in CuAl(11.5wt%)Ni(5.0wt%) single crystalline shape memory alloy", **Intermetallics**, 81 (2010) 1137. (IF.: 2.333).
- 4- **T.Y. El Rasasi**, L. Daróczy, D.L. Beke, "On the Chemical and Non Chemical Free Energies in the martensite transformation in Cu Al-Ni shape memory alloy" ,**ACTA PHYSICA DEBRECINA**, TOMUS XLIV (2010) 149. (IF.: 0.000)
- 5- **T.Y. El Rasasi**, M.M. Dobróka, L. Daróczy, D.L. Beke "Effect of thermal and mechanical cycling on the elastic and dissipative energy in CuAl(11,6wt%)Be(0.36wt%) shape memory alloy" in print in **Journal of Alloys and Compounds**. (IF. 2.134)
- 6- **T.Y. El Rasasi**, L. Daróczy, D.L. Beke "Calculation of elastic energy contributions in single crystalline Cu-11.5wt%Al-5.0wt%Ni shape memory alloy" submitted to **Materials Science Forum** (IF.: 0.000)
- 7- D.L. Beke, L. Daróczy, **T.Y. El Rasasi**, "Determination of the elastic and dissipative energy contributions to the martensitic phase transformation in shape memory alloys" accepted as a chapter in the book "**Shape memory Alloy**" book editor **F.M.B. Fernandes**, **IN TECH**, 2012

Citations:

- [1] M. Fischlschweiger, E.R. Oberaigner, "Kinetics and rates of martensitic phase transformation based on statistical physics", **Computational Materials Science** 52 (1) (2012) 189
- [2] Oberaigner, E.R., Fischlschweiger, M. "A statistical mechanics approach describing martensitic phase transformation" **Mechanics of Materials** 43 (9) (2012) 467

Posters:

[P1] Poster in the *ESOMAT 2009*,

"On the temperature and stress dependence of transformation strain in single crystalline Cu-Al-Ni shape memory alloys".

D.L. Beke, T.Y. El Rasasi, L. Daróczy,

[P2] Poster in the *VII Hungarian Conference on Material Science 2009*,

"On the relation between the martensite start stress and the temperature in single crystalline Cu-11.5wt%Al-5.0wt%Ni shape memory alloy".

T.Y. El Rasasi, L. Daróczy, D.L. Beke

[P3] Poster and oral presentation in *The 1st Egyptian Scientific workshop, Vienna 2011* *"On the Chemical and Non Chemical Free Energies in the martensite transformation in Cu Al-Ni shape memory alloy"*.

T.Y. El Rasasi, L. Daróczy, D.L. Beke

[P4] Poster in the *ICOMAT 2011 Osaka, Japan 2011*

"Effect of thermal and mechanical cycling on the elastic and dissipative energy in CuAl(11,6wt%)Be(0.36wt%) shape memory alloy".

T.Y. El Rasasi, M.M. Dobróka, L. Daróczy, D.L. Beke

[P5] Poster in the *VIII Hungarian Conference on Materials Science 2011*

"Calculation of elastic energy contributions as the function of the martensite volume fraction in single crystalline Cu-11.5wt%Al-5.0wt%Ni shape memory alloy".

T.Y. El Rasasi, L. Daróczy, D.L. Beke

[P6] Oral presentation in *The 2^{ed} Egyptian Scientific workshop, Prague 2012*

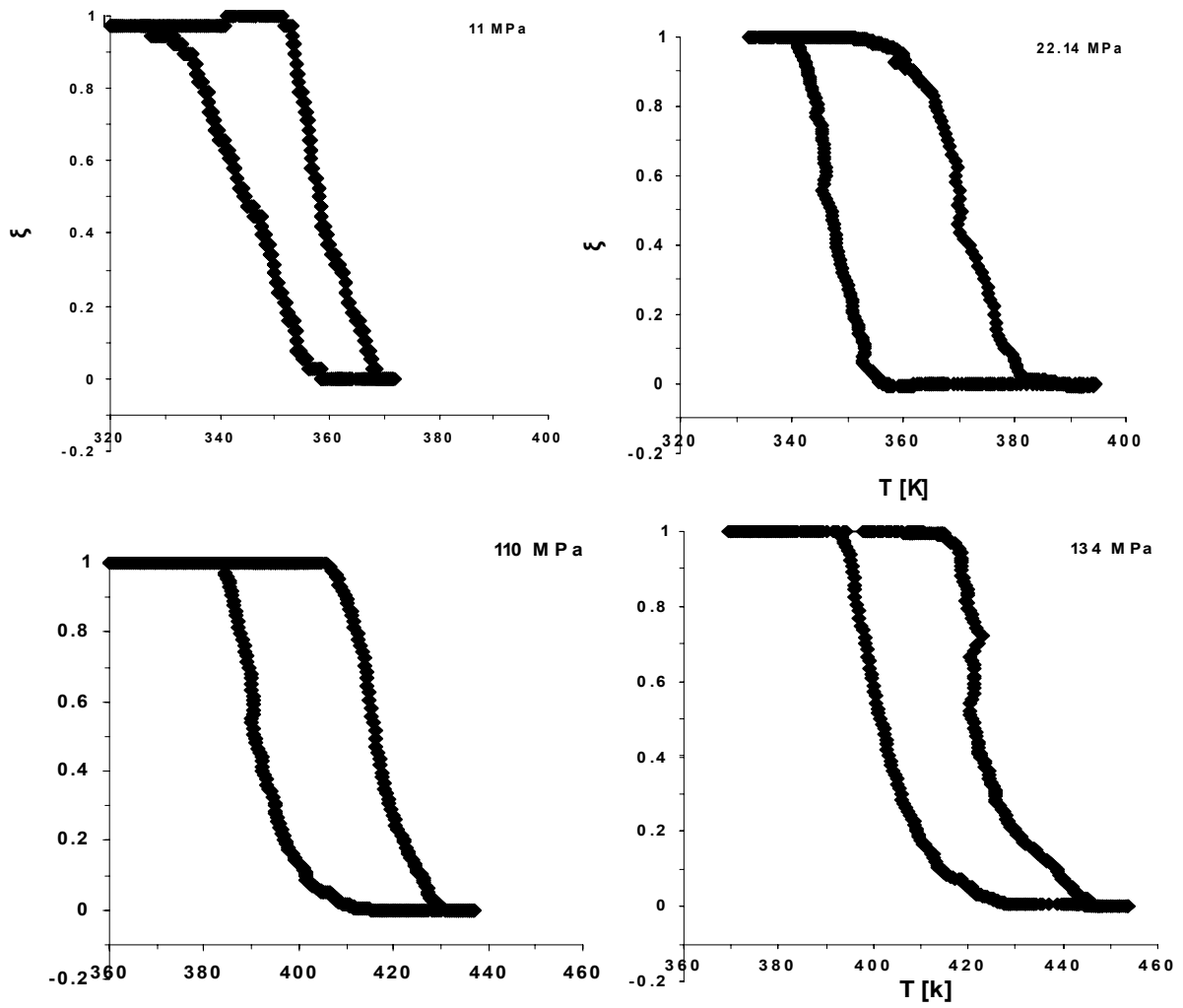
"On the elastic and dissipative energy contributions to the phase transformations in Cu-based shape memory alloys".

T.Y. El Rasasi, L. Daróczy, D.L. Beke

Appendices

Appendix I

Normalized hysteresis curves of the ε -T curves at 4 different applied stresses



Acknowledgments

First of all I would like to thank my supervisor Professor Dezső Beke deeply for giving me the opportunity to work in the very interesting area of shape memory alloys at the Department of Solid State Physics. In particular, I would like to thank him for sharing his ideas and knowledge with me, and helping me in all ways.

I would also like to thank Dr. Lajos Daróczi he has taught me for a lot of things that helped me in doing the experiments, and I think that I will be able to construct what I want using his ideas.

I would like to thank every one in the Department of Solid State Physics, I felt that this department is like one family, and I felt that I am one member of this kind family.

Many thanks for all my friends and colleagues they played a very important rule in my life.

At the last, I would like to thank also my family for supporting me throughout all that years.

The work is supported by the TÁMOP-4.2.2/B-10/1-2010-0024 project.

The project is co-financed by the European Union and the European Social Fund.

And also supported by the Hungarian Scientific Research Fund (OTKA) project No.

K 84065